AJRCCM Articles in Press. Published on 29-June-2017 as 10.1164/rccm.201603-0568OC

Differential expression of VEGF-A_{xxx} isoforms is critical for development of Pulmonary Fibrosis

Authors: Shaney L.Barratt[1], Thomas Blythe[1], Caroline Jarrett[1], Khadija Ourradi[1], Golda Shelley-Fraser[2], Michael J.Day[3], Yan Qiu[4], Steve Harper[4], Toby M.Maher[5], Sebastian Oltean[6], Thomas J.Hames[7], Chris J.Scotton[7], Gavin I.Welsh[4], David O.Bates[8], Ann B.Millar[1*]

Affiliations:
1. Academic Respiratory Unit, School of Clinical Sciences, University of Bristol, Bristol, UK.
2. Department of Histopathology, Cheltenham and Gloucestershire NHS Trust, Cheltenham, UK.
3. School of Veterinary Sciences, University of Bristol, Bristol, UK.
4. Academic Renal Unit, Bristol University, Bristol, UK.
5. NIHR Respiratory Biomedical Research Unit, Royal Brompton Hospital, London, UK.
6. Department of Physiology and Pharmacology, University of Bristol, Bristol, UK.
7. University of Exeter Medical School, Exeter, UK.
8. Cancer Biology, Division of Cancer and Stem cells, School of Medicine, University of Nottingham, Nottingham, UK.

*Correspondence should be addressed to Ann.millar@bristol.ac.uk

(t) 00441173235348 (f) 00441173235018

Author contributions: SLB, SO, CJS, GIW, DB and ABM designed and carried out experiments, TB,TH, CJ, KO, GS-F, MJD, SH carried out experiments, TM contributed samples and YQ developed the MMTV mouse line. SLB, GIW, CJS, DB and ABM analysed the data and wrote the manuscript

Funding: This work was supported by the Wellcome trust (grant numbers 95114) and the Richard Bright VEGF Research Trust.

Running Head VEGF and IPF

This article has an online data supplement, which is accessible from this issue's table of content online at www.atsjournals.org

AT A GLANCE COMMENTARY:

Scientific Knowledge on the subject: Failure of tissue repair leads to fibrosis and organ dysfunction and is an increasing cause of disease. Idiopathic pulmonary fibrosis (IPF) is an exemplar of this process in which Vascular Endothelial Growth Factor-A (VEGF-A) has been pathogenically implicated.

What this study adds to the field: We show that IPF is associated with an increased expression of an inhibitory VEGF-A splice variant (VEGF-A_{165}b) in IPF lung tissue, isolated IPF lung fibroblasts and plasma of IPF patients with progressive disease. In a mouse model of pulmonary fibrosis alveolar type II cell (ATII) specific deficiency of VEGF-A or constitutive over-expression of VEGF-A_{165}b inhibited the development of pulmonary fibrosis, as did treatment with intra-peritoneal delivery of VEGF-A_{165}b to wild-type mice. These results indicate that changes in the bioavailability of VEGF-A sourced from ATII cells, namely the ratio of VEGF-A_{xxx}a to VEGF-A_{xxx}b, are critical in the development of pulmonary fibrosis and may be a paradigm for the regulation of tissue repair.

AJRCCM Articles in Press. Published on 29-June-2017 as 10.1164/rccm.201603-0568OC

ABSTRACT:

Rationale: Fibrosis following lung injury is related to poor outcome and Idiopathic Pulmonary Fibrosis (IPF) can be regarded as an exemplar. Vascular Endothelial Growth Factor-A (VEGF–A) has been implicated in this context but there are conflicting reports as to whether it is a contributory or protective factor. Differential splicing of the VEGF-A gene produces multiple functional isoforms including VEGF-A_{165}a, and VEGF-A_{165}b a member of the inhibitory family. To-date there is no clear information on the role of VEGF in IPF.

Objectives: To establish VEGF isoform expression and functional effects in IPF.

Methods: We used tissue sections, plasma and lung fibroblasts from IPF patients and controls. In a bleomycin-induced lung fibrosis model we used wild type MMTV mice and a triple transgenic mouse SPC-rtTA$^{+/-}$TetoCre$^{+/-}$LoxP-VEGF-A$^{+/+}$ to conditionally induce VEGF-A isoform deletion specifically in the ATII cells of adult mice.

Measurements and main Results: IPF and normal lung fibroblasts differentially expressed and responded to VEGF-A_{165}a and VEGF-A_{165}b, in terms of proliferation and matrix expression. Increased VEGF-A_{165}b was detected in sera of progressing IPF patients. In a mouse model of pulmonary fibrosis alveolar type II cell (ATII) specific deficiency of VEGF-A or constitutive over-expression of VEGF-A_{165}b inhibited the development of pulmonary fibrosis, as did treatment with intra-peritoneal delivery of VEGF-A_{165}b to wild-type mice.

Conclusions: These results indicate that changes in the bioavailability of VEGF-A sourced from ATII cells, namely the ratio of VEGF-A_{xxx}a to VEGF-A_{xxx}b, are critical in development of pulmonary fibrosis and may be a paradigm for the regulation of tissue repair.

Word Count: 250 **Keywords:** Idiopathic pulmonary fibrosis, Vascular endothelial Growth Factor (VEGF), animal models of pulmonary fibrosis

Introduction

Fibrosis in the lung or elsewhere is part of the normal repair mechanism following injury. Idiopathic pulmonary fibrosis (IPF) can be considered as a paradigm of an aberrant repair process in response to repeated and unidentified injury. IPF is a devastating progressive fibrosing lung disease of unknown cause that is increasing in incidence(1). Median survival is 3-5 years and treatment options are limited(2, 3), leading to an estimated mortality rate of more than 50 deaths per 1,000,000 persons in the US(4) and UK(1) .

Vascular Endothelial Growth Factor-A, originally described as an angiogenic factor, belongs to a super-family of glycoproteins, and signals through tyrosine kinase receptors VEGF receptor 1 (VEGFR1) and VEGF receptor 2 (VEGFR2) and co-receptors, neuropilins 1 and 2 (NP1 and NP2)(5, 6). However, VEGF biology has undergone radical revision since its discovery. It has been identified in primitive organisms that have no vasculature(7), is not specific to endothelial cells and is increasingly recognized as vital in the function and maintenance of non-endothelial cells(8, 9). *In vitro* studies have confirmed that VEGF-A is abundant in lung tissue, especially in alveolar epithelium(10-14) and has a role in lung development(15) and maturation(16). In the healthy lung processes classically associated with VEGF-A are extremely restricted(14, 17, 18). This apparent paradox has led to controversy about the role of VEGF-A in the normal and diseased lung(19).

Several pathogenic mechanisms for the development of IPF have been proposed but currently a form of recurrent alveolar type II (AT II) epithelial injury leading to aberrant collagen deposition from fibroblasts is most widely accepted(20). Evidence on the role of VEGF-A in IPF conflicts(21),(22),(23). Evidence that VEGF-A may facilitate fibrogenesis comes from the

AJRCCM Articles in Press. Published on 29-June-2017 as 10.1164/rccm.201603-0568OC

extensive trials of FDA approved nintedanib, a triple tyrosine kinase inhibitor, including the VEGFR2 receptor(24, 25). In contrast, several clinical studies have indicated a reparative role for VEGF-A in the lung (17, 18), with pre-clinical studies suggesting a protective role for VEGF-A against the development of excessive pulmonary fibrosis as a result of lung injury(26-28).

Differential splicing of the VEGF-A gene produces multiple functional isoforms (29) : proximal splice site selection with exon 8 produces the conventional family of VEGF-A_{xxx}a isoforms. Distal splice site selection within exon 8 produces an alternative family of isoforms (VEGF-A_{xxx}b family), that have the same number of amino acids as the conventional family in humans, but six different amino acids at the C terminus(30). The most widely studied of these isoforms, VEGF-A_{165}b, is functionally different from VEGF-A_{165}a(30, 31). VEGF-A_{165}b inhibits canonical VEGF-A signalling by competitive interference with conventional isoforms at the VEGFR2–NP1 receptor complex, preventing full downstream signalling by VEGFR2(32). Knowledge of inhibitory VEGF-A variants in clinical tissue repair syndromes is limited(33). We have shown that they inhibit VEGF-A_{165}a induced ATII and pulmonary microvascular proliferation in vitro(10). Functional Murine VEGF-A_{165}b has been described (33). Thus a number of regulatory events at the 3′ end of the VEGF-A gene are required for precise physiological control of VEGF-A bioavailability(34).

Hitherto, the vast majority of studies have examined VEGF as a single molecule. Differential expression of the numerous VEGF-A isoforms offers one explanation for the apparent discrepancies observed in the literature. In this study we have focused on the role of VEGF in relation to fibroblast function. We show that ATII cell-specific production of VEGF-A is a key checkpoint for controlling lung fibrogenesis. VEGF-A_{165}b acts as a natural regulator of this

process and has potential therapeutic applications for restoring homeostasis to the lung and treating fibrosis. Some of the results have been previously reported in abstract form(35-37).

Methods:

Human tissue collection

Anonymised human lung biopsies and bronchoalveolar lavage (BAL) were donated from patients undergoing clinically indicated procedures. The Bristol institutional review boards granted ethical approval. Additional IPF tissue and plasma samples came from the Lung Tissue Research Consortium (LTRC), USA, and Toby Maher (Royal Brompton Hospital, UK, (38)).

Primary lung fibroblast culture

Primary lung fibroblasts were explanted from lung biopsies as previously described or obtained from the American Type Culture Collection.

RT-PCR and Quantitative RT-PCR

Total RNA was extracted using the Quick RNA^{TM} kit (Zymo Research) and reverse transcribed with Taqman High Capacity RNA-to-cDNA kit (Applied Biosystems). Individual qRT-PCR reaction mixes were made using manufacturer recommendations (2x SensiFAST SYBR Hi-ROX (Bioline). Human and murine primer sets are in Tables E1 and E2. Expression of human VEGF-A_{xxx}a and VEGF-A_{xxx}b isoforms were also quantified (39).

Cell Immunofluorescence

Cells were fixed, permeabilised and blocked before incubation with primary antibody overnight and then secondary antibody before image capture.

AJRCCM Articles in Press. Published on 29-June-2017 as 10.1164/rccm.201603-0568OC

Western-Blot Analysis

Cell lysates were prepared using radioimmunoprecipitation buffer (Sigma,), containing protease and phosphatase inhibitor cocktails (Sigma). Lysates were fractionated, immunoblotted, blocked, then incubated with primary antibodies and loading controls. *High Performance Liquid Chromatography (HPLC)*

HPLC was used to quantify fibroblast collagen production (40).

Immunohistochemistry

Slides were de-waxed before rehydration and antigen retrieval. Endogenous peroxidases were blocked and sections incubated with primary antibody or IgG control.

ELISA of PanVEGF-A and VEGF-$A_{165}b$

PanVEGF-A and VEGF-A_{165}b levels were quantified using PanVEGF-A and VEGF-A_{165}b ELISA sets (R&D systems).

Cell Proliferation assay and wound healing –migration Assay

Fibroblasts were seeded into 24-well plates or IBIDI culture chambers, quiesced and following stimulation, counted or imaged.

Animal housing and breeding

All experiments were carried out in accordance with the UK Animals (Scientific Procedures) Act 1986 and University of Bristol ethical review panel approval. TG mice constitutively over-expressing VEGF-A_{165}b (MMTV-$VEGF_{165}b^{+/-}$) were generated as previously described(41). SPC-$rtTA^{+/-}$Tet-O-$Cre^{+/-}$LoxP $VEGF^{+/+}$ mice were generated on C57Bl6 background by crossing three transgenic mouse lines: LoxP-VEGF (Genentech, San Franscisco, USA(42), Cre-recombinase, under control of a tetracycline-responsive promoter element (Tet-O) and TG mice

expressing the reverse tetracycline-controlled transactivator (rtTA) protein under control surfactant, pulmonary-associated protein C, promoter(SPC)(Jackson)(43).

Animal studies

The Bleomycin-induced model of pulmonary fibrosis was used (44). Lung fibrosis was assessed by fibronectin and pro-collagen-1α mRNA expression and histologically by Masson's Trichrome staining and lung fibrosis score.

Further experimental details are available on line.

Statistical analysis

Statistical analysis was performed using Graph Pad Prism software (Version 5.0). Unpaired *t*-test was used, with or without Welch's correction dependent on the variance of data. ANOVA with post-hoc Holm's Sidak multiple comparisons analysis was used for multiple comparisons. For all tests a $p < 0.05$ was considered statistically significant.

Results

PanVEGF-A and VEGF-A_{xxx}b expression in IPF patients

Whole lung tissue expression of panVEGF-A (collective VEGF- A isoforms), VEGF-A_{xxx}b, VEGF-A_{121}a, VEGF-A_{165}a and VEGF-A_{189}a was detected at mRNA level (**Figure 1a**), confirmed by sequencing (**Figure E 1**) and quantified (**Figure 1b**). PanVEGF-A protein levels in whole lung were comparable between normal and IPF, but intriguingly VEGF-A_{165}b protein expression was dramatically increased in IPF lung tissue (**Figure 1c).** VEGF-A_{165}b, but not panVEGF-A in

AJRCCM Articles in Press. Published on 29-June-2017 as 10.1164/rccm.201603-0568OC

baseline plasma samples of subsequent progressors (death or >10% decline in FVC at 12 months) were significantly greater than non-progressors (**Figure 1d**).

Levels of VEGF-A (representing only the soluble isoforms, VEGF-A_{121} and VEGF-A_{165}), investigated by pan-VEGF-A ELISA, were significantly lower in bronchoalveolar lavage fluid (BALF) of IPF patients compared to controls (**Figure 1e**), as previously reported (13, 45-47). Patient demographics were comparable (**Figure E 2a**). VEGF-A_{165}b was undetectable in BALF, using an ELISA specific for an epitope encoded by exon 8b suggesting it was not secreted into an area accessible by this procedure or was below the detection limit (10pg/ml). Using immunohistochemistry, we found that in both normal and IPF lung panVEGF-A and VEGF-A_{165}b were prominent within alveolar epithelium (AEC) (**Figure 1f and Figure E2b**) but also localised to macrophages, lymphocytes and fibroblasts, particularly outside the fibrotic focus. These data suggest that there is an increased expression of VEGF-A_{165}b in IPF, one source being ATII cells as previously shown in normal lung(10). To understand the biological potential of these findings in IPF we investigated the expression of the receptors and co-receptors necessary for functional activity.

VEGF receptor and co-receptors in IPF patients

Expression of VEGFR1, VEGFR2, NP1 and NP2 was detected at the mRNA level in normal and IPF lung whole lung tissue (**Figure 2a**). Expression of VEGFR1 and NP1 was significantly up-regulated in IPF lung.

Using immunohistochemistry, we found that in normal and IPF lung VEGFR1, VEGFR2, NP1 and NP2 were expressed on AEC, macrophages, lymphocytes and fibroblasts surrounding fibrotic foci with reduced expression within the foci (**Figure 2b and Figure E 3A**).

Lung whole tissue lysates expressed VEGFR1, VEGFR2, NP1 and NP2 protein (**Figure 2c**). There was a significant reduction in protein expression of VEGFR1 in the whole IPF lung samples (fibrotic foci and surrounding tissue) with a trend to reduced VEGFR2 and NP1. Co-staining of VEGFR1 and VEGFR2 with epithelial-specific E-Cadherin suggests that non-endothelial cells are VEGF-A targets (**Figure E 3B**).

These data demonstrated the potential for VEGF-A to have functional effects in fibrotic lung. In this context, we then looked at isolated fibroblast cultures, the potential effector cells, from IPF and normal subjects.

VEGF-A receptors and co-receptors are expressed by primary lung fibroblasts and VEGF-A stimulation stimulates downstream signaling pathways

VEGFR1, VEGFR2, NP1 and NP2 were endogenously expressed by fibroblasts from normal subjects (NF) and IPF patients (FF), at the mRNA level (**Figure E 3C**). FF expressed less VEGFR1 and NP2 protein (**Figure 3a**). Surprisingly, these cells did not express mature VEGFR2 protein by western blotting. These results were corroborated by ELISA; the expression of VEGFR2 was below the detection limit (≤30pg/ml). VEGFR2 is conventionally considered the main signalling receptor so we investigated whether signalling could occur**.** Treatment of NF and FF cultures with rhVEGF-A_{165}a or rhVEGF-A_{165}b proteins led to increased phosphorylation of MEK1/2 (Mitogen/Extracellular signal related Kinase) and p42/44 MAPK (Mitogen Activated Protein Kinase) proteins (**Figure 3b and Figure E 4**).

AJRCCM Articles in Press. Published on 29-June-2017 as 10.1164/rccm.201603-0568OC

VEGF-A isoforms are expressed in primary lung fibroblasts

NF and FF were characterized as expressing three major VEGF-A isoforms detectable at the RNA level by RT-PCR and confirmed by sequencing (**Figure E 5 and E 6).** Comparable levels of panVEGF-A and VEGF-A_{xxx}b mRNA were demonstrated in NF and FF by qRT-PCR (**Figure E 7**).

In contrast, comparable protein expression of panVEGF-A, but increased expression of VEGF-A_{xxx}b isoforms in FF cell lysates was identified by western blotting (**Fig 3c**). Quantification of panVEGF-A and VEGF-A_{xxx}b protein expression in cell lysates of NF and FF cultures by ELISA supported these findings (**Figure 3d**).

Localisation of panVEGF-A and VEGF-A_{165}b expression by immunofluorescence demonstrated cytoplasmic localisation in all NF and FF, with additional panVEGF-A perinuclear staining (**Figure 3e and Figure E 8)**. These data suggest an additional potential for autocrine effects of panVEGF-A and VEGF-A_{165}b on fibroblasts.

Having shown the potential for functional effects of VEGF-A_{165}a and VEGF-A_{165}b on fibroblasts we then explored how they might relate to IPF pathology.

VEGF-A_{165}a and VEGF-A_{165}b recombinant proteins have differential effects on fibroblast proliferation, migration and ECM expression

We examined fibroblastic fibronectin and collagen expression (**Figure 4a-c**). Administration of rhVEGF-A_{165}a significantly increased protein expression of fibronectin but not collagen by NF and FF. No significant effect was observed for either protein following rhVEGF-A_{165}b administration **(Fig. 4a,c)**. However, with increasing levels of VEGF-A_{165}b, the VEGF-A_{165}a-induced increase in fibronectin was inhibited, an effect more apparent for FF **(Figure 4b).** In the

presence of both isoforms, VEGF-A_{165}b inhibited collagen production in NF but not FF **(Figure 4c)**.

Recombinant VEGF-A_{165}a also significantly increased the proliferation of FF, inhibited by the concomitant addition of VEGF-A_{165}b **(Figure 4d)**. Concomitant treatment of NF with VEGF-A_{165}a and VEGF-A_{165}b inhibited cell proliferation compared to VEGF-A_{165}a alone.

Furthermore, VEGF-A_{165}a and VEGF-A_{165}b significantly increased NF migration. This effect was blocked by the concomitant treatment of VEGF-A_{165}a and VEGF-A_{165}b. In contrast, recombinant VEGF-A proteins had no significant effect on FF migration **(Figure 4e and Figure E 9)**.

Collectively these data supported an *in-vitro* mechanism by which VEGF-A_{165}a could induce a fibrotic response ameliorated by VEGF-A_{165}b. In the context of IPF, VEGF-A_{165}b could ameliorate the development of IPF with ATII cells as the predominant source and fibroblasts as the likely effector cells, so to consider this in more detail we turned to an animal model.

Alveolar epithelial expression of VEGF-A_{xxx}a is essential for development of pulmonary fibrosis.

To determine the effect of VEGF-A on the development of Bleomycin (BLM)-induced pulmonary fibrosis(44), we generated a triple transgenic mouse SPC-rtTA$^{+/-}$TetoCre$^{+/-}$LoxP-VEGF-A$^{+/+}$ (termed STCLL) on a C57Bl/6 background to conditionally induce the deletion of VEGF-A isoforms specifically in the ATII cells of adult mice. Tissue specificity of Cre-recombinase activity following doxycycline induction was confirmed by *in-vivo* imaging of doxycycline induced GFP-SPC-rtTA$^{+/-}$TetoCre$^{+/-}$LoxP-VEGF-A$^{+/-}$ mice (termed GFP-STCL) (**Figure 5a and Figure E 10**). Quantitative RT-PCR of whole lung tissue RNA extracts demonstrated reduced panVEGF-A in doxycycline induced TG mice. *In situ* hybridisation,

AJRCCM Articles in Press. Published on 29-June-2017 as 10.1164/rccm.201603-0568OC

indicated a lack of VEGF-A mRNA in the murine ATII cells and panVEGF-A immunohistochemistry corroborated findings of reduced ATII-derived VEGF-A **(Figure 5a**).

Deletion of ATII VEGF-A, significantly reduced the development of BLM-induced pulmonary fibrosis by both a blindly assessed lung fibrosis score and reduced collagen deposition and architectural distortion (**Figure 5b**). Furthermore, lung fibronectin mRNA expression was significantly reduced in BLM-treated STCLL mice compared to BLM-treated WT controls, with a trend towards a reduction in pro-collagen-1α mRNA levels in these TG mice (**Figure 5b**). This demonstrates that ATII expression of VEGF-A is required for fibrosis to occur.

VEGF-A_{165}b may be protective against the formation of pulmonary fibrosis

A TG mouse that over-expresses VEGF-A_{165}b using a MMTV promoter as a driver of expression has been described(41). This mouse has increased levels of the MMTV-VEGF-A_{165}b transgene and human VEGF-A_{165}b in the lung (**Figure E 11a)**. H&E stained lung sections of TG mice were histologically normal, in particular with no vascular abnormalities, as might be expected in view of the established compartmentalization of lung VEGF(14) (**Figure E 11b**). IHC staining of TG mouse lung sections demonstrated increased VEGF-A_{165}b expression localized to alveolar epithelial cells, compared to both mouse IgG and WT controls (**Figure 6a**). Homogenized lung tissue extracts from MMTV-VEGF-A_{165}b mice expressed significantly more VEGF-A_{165}b protein than littermate WT controls by ELISA, with detectable VEGF-A_{165}b levels in BALF of TG mice, but below the detection limit of the ELISA in WT controls (**Figure 6a**).

In this pre-clinical model the development of pulmonary fibrosis was significantly reduced in TG mice compared to WT mice (**Figure 6b**). Pro-collagen-1α mRNA levels were significantly reduced in BLM-treated TG mice compared to BLM-treated WT littermates, with a trend to reduction in fibronectin mRNA in these same TG mice **(Figure 6b)**. These data show a

protective effect of VEGF-A_{165}b within the lung when expressed particularly by the alveolar epithelium, supporting a potential for therapeutic application.

To determine the effect of VEGF-A_{165}b on the development of BLM-induced pulmonary fibrosis, WT C57/Bl/6 mice received oro-pharyngeal (OP) BLM with or without the additional intra-peritoneal (IP) delivery of rhVEGF-A_{165}b. Importantly, in one arm of the study, to specifically address the potential therapeutic benefit of VEGF-A_{165}b, the compound was delivered during the fibrotic rather than the inflammatory phase of the model (late VEGF-A_{165}b group).

IP injection of VEGF-A_{165}b significantly reduced the development of pulmonary fibrosis in WT mice. This protective effect of VEGF-A_{165}b was evident in the early VEGF-A_{165}b (EV) and late VEGF-A_{165}b (LV) groups suggesting a protective effect of VEGF-A_{165}b (**Figure 6c**). Whilst the expression of fibronectin and pro-collagen-1α mRNA in whole lung tissue RNA extracts was significantly up-regulated in mice treated with BLM + Saline IP, the expression in both VEGF-A_{165}b IP groups was not significantly different from OP Saline-treated controls, supporting the notion that VEGF-A_{xxx}a is pro-fibrotic and VEGF-A_{xxx}b is protective.

DISCUSSION

Whilst VEGF-A has been implicated in the response of the lung to injury there are conflicting reports as to whether it functions as a contributory or protective factor(21, 22, 27, 28). Processes classically associated with VEGF-A are extremely restricted within the normal lung (14, 17, 18) which reflects the increasing recognition of VEGF as vital in the function and maintenance of non-endothelial cells (8, 9). Cumulative evidence from several studies has suggested that the alternatively spliced VEGF-A_{xxx}b isoforms may have opposing/inhibitory functions compared to

AJRCCM Articles in Press. Published on 29-June-2017 as 10.1164/rccm.201603-0568OC

the conventional VEGF-A_{xxx}a family(31) and appreciation of the existence of numerous VEGF-A isoforms and their interaction with VEGF-A receptors and co-factors determining VEGF-A bioavailability, offers one potential explanation for these discrepant findings.

We show that differential expression of VEGF-A_{xxx}a and VEGF-A_{xxx}b isoforms in the IPF lung can result in functional changes to the fibrotic process, and that ATII cell VEGF-A is critical for the development of fibrosis in a pre-clinical murine model. The finding that in this model fibrosis can be prevented or resolved by expression of the inhibitory isoform indicates that it is the VEGF-A_{xxx}a family that is pro-fibrotic and the VEGF-A_{xxx}b family is inhibitory/regulatory. This leads to two potential new therapeutic approaches for IPF – selective inhibition of VEGF-A_{xxx}a or stimulation (or administration) of VEGF-A_{165}b. The development of a specific VEGF-A_{165}a antibody (48, 49) and small molecule splicing agents which alter the relative balance of VEGF-A isoforms (50, 51), could facilitate this.

We have shown significant up-regulation of VEGF-A_{165}b within IPF lung tissue compared to normal lung. This was particularly seen in both ATII cells and fibroblasts (outside the fibrotic foci) in the most severely fibrotic areas of the IPF. These data were obtained from patients with established disease suggesting that dysregulated fibrosis has occurred despite these changes. We speculate that the increase in VEGF-A_{165}b is a compensatory mechanism that was insufficient to prevent inappropriate fibrosis in these patients, however in some patients at risk, fibrosis will be prevented. Sequential lung tissue data to support this is not available as these patients present with established disease. However, increased VEGF-A_{165}b in baseline plasma samples from patients with subsequent progression supports this hypothesis(38). In contrast, we found a significant reduction in panVEGF-A expression in the BALF of IPF patients by ELISA as previously observed (45-47) and VEGF-A_{165}b levels were undetectable in identical BALF

samples. The nature of BALF collection from IPF lung would favour least affected areas and the greatest intensity of immunohistochemical staining for VEGF-A_{165}b was in the most fibrotic areas.

The isoform production switch, altering the ratio of VEGF-A_{xxx}a to VEGF-A_{xxx}b could be viewed as a contributor to disease, or as a protective response of the ATII and other cells, a regulatory mechanism to maintain homeostasis as we have previously postulated in the lung(10) and others in systemic sclerosis(52, 53). Interestingly, it has become clear that IPF is associated with multiple splicing changes, such as that required for VEGF-A_{165}b(54, 55).

VEGFR1 was down-regulated in IPF and expression was low in fibrotic fibroblasts, with additional trends towards a reduction in both VEGFR2 and NP1 expression in IPF. This may be due to the presence of increased VEGF-A_{165}b that has been shown to cause down-regulation of VEGFR2, as it results in internalisation and degradation through the endosomal pathway(32). Although fibroblasts lack VEGFR2, historically considered the most biologically active of all the VEGF receptors(56), we demonstrated that recombinant VEGF-A proteins have differential effects on the proliferation, migration and ECM protein expression by these cells. Given that VEGF-A_{165}b levels are raised in IPF, and VEGF-A_{165}a stimulates pro-fibrotic effects in fibrotic fibroblasts, which were inhibited by VEGF-A_{165}b, this could be a protective mechanism in IPF that is being overwhelmed by the other inflammatory processes being driven forward (57). VEGF-A has been shown to have both paracrine and autocrine effects on several cell types within the lung (6) (10, 15) (16). It is our opinion that whilst the statistically significant differences observed in fibroblast responses to VEGF-A isoforms might appear biologically modest, they could have important implications in a slowly progressive fibrosing disease such as IPF, in which tissue remodelling and disease progression is best observed over months and years.

AJRCCM Articles in Press. Published on 29-June-2017 as 10.1164/rccm.201603-0568OC

Whilst *in vitro* studies utilizing co-cultures of IPF-derived alveolar epithelium and fibroblasts would be desirable to further study this mechanism, there are several recognized practical limitations to culturing IPF epithelial cells (58).

In our initial studies of a pre-clinical pulmonary fibrosis model we sought to determine the critical source of VEGF-A. We demonstrated a significant amelioration of the fibrotic response in a specific doxycycline induced ATII cell VEGF-A deficient mouse showing that alveolar production of VEGF-A is required for fibrosis to occur. VEGFA was not completely absent in this model, which is likely to reflect the situation in the human lung. We did not find any evidence of vascular abnormalities in our model though functional vascular studies were not undertaken. This supports the widely accepted notion in the pathogenesis of IPF that is of initiation by recurrent epithelial injury(20).

Using this same pre-clinical model, we explored the potential therapeutic benefit of IP rhVEGF-A_{165}b administration. The BLM-model of lung fibrosis has been characterized as having an early partially inflammatory phase followed by a fibrotic phase(44). In our study both early IP VEGF-A_{165}b and critically late IP VEGF-A_{165}b, delivered specifically in the 'fibrotic phase' of the fibrosis model, resulted in significant amelioration of pulmonary fibrosis. In conjunction with the previous data this demonstrates that it is VEGF-A_{xxx}a isoforms that are required for fibrosis.

This data supports our hypothesis that the co-ordinated expression of VEGF-A_{xxx}a and VEGF-A_{xxx}b isoforms is important in the development and progression of pulmonary fibrosis. Differential expression of these families of VEGF-A isoforms may explain, in part, some apparently contradictory studies describing VEGF-A as both a protective and contributory factor

in fibrogenesis. We describe for the first time the apparent protective effects of VEGF-A_{xxx}b expression in pre-clinical models of pulmonary fibrosis, an effect that may occur due to differential effects on fibroblastic synthetic function. Our findings support a 'non-angiogenic/non vascular' role for VEGF-A in the fibrotic lung. Future studies are required to elucidate further mechanisms by which VEGF-A_{xxx}b may inhibit fibrogenesis and to address factors that may regulate alternative splicing of the VEGF-A gene.

Acknowledgments:

We would like to thank Andrea Cupp (University of Nebraska) for the MMTV-$VEGF_{165}$b mice, S.Quaggin (University of Chicago) for reagents and mice, R. Coward (University of Bristol) for GFP reporter mouse and Genentech Inc for loxp-VEGF mice and the Lung Tissue Research Consortium for lung tissue samples.

AJRCCM Articles in Press. Published on 29-June-2017 as 10.1164/rccm.201603-0568OC

References

1. Navaratnam V, Fleming KM, West J, Smith CJ, Jenkins RG, Fogarty A, et al. The rising incidence of idiopathic pulmonary fibrosis in the U.K. *Thorax* 2011;66(6):462-7.
2. Collard HR, King TE, Jr., Bartelson BB, Vourlekis JS, Schwarz MI, Brown KK. Changes in clinical and physiologic variables predict survival in idiopathic pulmonary fibrosis. *Am J Respir Crit Care Med* 2003;168(5):538-42.
3. Raghu G, Weycker D, Edelsberg J, Bradford WZ, Oster G. Incidence and prevalence of idiopathic pulmonary fibrosis. *Am J Respir Crit Care Med* 2006;174(7):810-6.
4. Olson AL, Swigris JJ, Lezotte DC, Norris JM, Wilson CG, Brown KK. Mortality from pulmonary fibrosis increased in the United States from 1992 to 2003. *Am J Respir Crit Care Med* 2007;176(3):277-84.
5. Ferrara N. Vascular endothelial growth factor: basic science and clinical progress. *Endocr Rev* 2004;25(4):581-611.
6. Leung DW, Cachianes G, Kuang WJ, Goeddel DV, Ferrara N. Vascular endothelial growth factor is a secreted angiogenic mitogen. *Science* 1989;246(4935):1306-9.
7. Zacchigna S, Lambrechts D, Carmeliet P. Neurovascular signalling defects in neurodegeneration. *Nat Rev Neurosci* 2008;9(3):169-81.
8. Harper SJ, Bates DO. VEGF-A splicing: the key to anti-angiogenic therapeutics? *Nat Rev Cancer* 2008;8(11):880-7.
9. Bates DO. Vascular endothelial growth factors and vascular permeability. *Cardiovascular Research* 2010;87(2):262-71.
10. Varet J, Douglas SK, Gilmartin L, Medford AR, Bates DO, Harper SJ, et al. VEGF in the lung: a role for novel isoforms. *Am J Physiol Lung Cell Mol Physiol* 2010;298(6):L768-74.
11. Berse B, Brown LF, Van de Water L, Dvorak HF, Senger DR. Vascular permeability factor (vascular endothelial growth factor) gene is expressed differentially in normal tissues, macrophages, and tumors. *Mol Biol Cell* 1992;3(2):211-20.
12. Boussat S, Eddahibi S, Coste A, Fataccioli V, Gouge M, Housset B, et al. Expression and regulation of vascular endothelial growth factor in human pulmonary epithelial cells. *Am J Physiol Lung Cell Mol Physiol* 2000;279(2):L371-8.
13. Koyama S, Sato E, Tsukadaira A, Haniuda M, Numanami H, Kurai M, et al. Vascular endothelial growth factor mRNA and protein expression in airway epithelial cell lines in vitro. *Eur Respir J* 2002;20(6):1449-56.
14. Kaner RJ, Crystal RG. Compartmentalization of vascular endothelial growth factor to the epithelial surface of the human lung. *Mol Med* 2001;7(4):240-6.
15. Brown KR, England KM, Goss KL, Snyder JM, Acarregui MJ. VEGF induces airway epithelial cell proliferation in human fetal lung in vitro. *Am J Physiol Lung Cell Mol Physiol* 2001;281(4):L1001-10.
16. Compernolle V, Brusselmans K, Acker T, Hoet P, Tjwa M, Beck H, et al. Loss of HIF-2alpha and inhibition of VEGF impair fetal lung maturation, whereas treatment with VEGF prevents fatal respiratory distress in premature mice. *Nat Med* 2002;8(7):702-10.
17. Thickett DR, Armstrong L, Christie SJ, Millar AB. Vascular endothelial growth factor may contribute to increased vascular permeability in acute respiratory distress syndrome. *Am J Respir Crit Care Med* 2001;164(9):1601-5.
18. Thickett DR, Armstrong L, Millar AB. A role for vascular endothelial growth factor in acute and resolving lung injury. *Am J Respir Crit Care Med* 2002;166(10):1332-7.

19. Medford AR, Millar AB. Vascular endothelial growth factor (VEGF) in acute lung injury (ALI) and acute respiratory distress syndrome (ARDS): paradox or paradigm? *Thorax* 2006;61(7):621-6.
20. Sakai N, Tager AM. Fibrosis of two: Epithelial cell-fibroblast interactions in pulmonary fibrosis. *Biochim Biophys Acta* 2013;1832(7):911-21.
21. Hamada N, Kuwano K, Yamada M, Hagimoto N, Hiasa K, Egashira K, et al. Anti-vascular endothelial growth factor gene therapy attenuates lung injury and fibrosis in mice. *J Immunol* 2005;175(2):1224-31.
22. Ou XM, Li WC, Liu DS, Li YP, Wen FQ, Feng YL, et al. VEGFR-2 antagonist SU5416 attenuates bleomycin-induced pulmonary fibrosis in mice. *Int Immunopharmacol* 2009;9(1):70-9.
23. Farkas L, Farkas D, Ask K, Moller A, Gauldie J, Margetts P, et al. VEGF ameliorates pulmonary hypertension through inhibition of endothelial apoptosis in experimental lung fibrosis in rats. *J Clin Invest* 2009;119(5):1298-311.
24. Chaudhary NI, Roth GJ, Hilberg F, Muller-Quernheim J, Prasse A, Zissel G, et al. Inhibition of PDGF, VEGF and FGF signalling attenuates fibrosis. *Eur Respir J* 2007;29(5):976-85.
25. Richeldi L, du Bois RM, Raghu G, Azuma A, Brown KK, Costabel U, et al. Efficacy and safety of nintedanib in idiopathic pulmonary fibrosis. *N Engl J Med* 2014;370(22):2071-82.
26. Kearns MT, Dalal S, Horstmann SA, Richens TR, Tanaka T, Doe JM, et al. Vascular endothelial growth factor enhances macrophage clearance of apoptotic cells. *Am J Physiol Lung Cell Mol Physiol* 2012;302(7):L711-8.
27. Stockmann C, Kerdiles Y, Nomaksteinsky M, Weidemann A, Takeda N, Doedens A, et al. Loss of myeloid cell-derived vascular endothelial growth factor accelerates fibrosis. *Proc Natl Acad Sci U S A* 2010;107(9):4329-34.
28. Lee S, Chen TT, Barber CL, Jordan MC, Murdock J, Desai S, et al. Autocrine VEGF signaling is required for vascular homeostasis. *Cell* 2007;130(4):691-703.
29. Houck KA, Leung DW, Rowland AM, Winer J, Ferrara N. Dual regulation of vascular endothelial growth factor bioavailability by genetic and proteolytic mechanisms. *J Biol Chem* 1992;267(36):26031-7.
30. Bates DO, Cui TG, Doughty JM, Winkler M, Sugiono M, Shields JD, et al. VEGF165b, an inhibitory splice variant of vascular endothelial growth factor, is down-regulated in renal cell carcinoma. *Cancer Res* 2002;62(14):4123-31.
31. Woolard J, Wang WY, Bevan HS, Qiu Y, Morbidelli L, Pritchard-Jones RO, et al. VEGF165b, an inhibitory vascular endothelial growth factor splice variant: mechanism of action, in vivo effect on angiogenesis and endogenous protein expression. *Cancer Res* 2004;64(21):7822-35.
32. Ballmer-Hofer K, Andersson AE, Ratcliffe LE, Berger P. Neuropilin-1 promotes VEGFR-2 trafficking through Rab11 vesicles thereby specifying signal output. *Blood* 2011;118(3):816-26.
33. Kikuchi R, Nakamura K, MacLauchlan S, Ngo DT, Shimizu I, Fuster JJ, et al. An antiangiogenic isoform of VEGF-A contributes to impaired vascularization in peripheral artery disease. *Nat Med* 2014;20(12):1464-71.
34. Eswarappa SM, Potdar AA, Koch WJ, Fan Y, Vasu K, Lindner D, et al. Programmed translational readthrough generates antiangiogenic VEGF-Ax. *Cell* 2014;157(7):1605-18.

AJRCCM Articles in Press. Published on 29-June-2017 as 10.1164/rccm.201603-0568OC

35. Barratt SL JC, Blythe T, Welsh GI, Maher T, Bates DO, Millar AB. Bioavailability ofVEGF in idiopathic pulmonary fibrosis. *Thorax* 2012;67(Suppl2) doi:10.1136/thoraxjnl-2012-202678.074. Unpublished paper.
36. Barratt SL, Blythe T, Jarrett C, Welsh GI, Ourradi K, Scotton CS, Bates DO, and Millar AB. Vascular Endothelial Growth Factor (VEGF) Expression in the IPF Lung – A role for anti-angiogenic isoforms? *Thorax* 2014;69(Suppl2) http://dx.doi.org/10.1136/thoraxjnl-2014-206260.143. Unpublished paper.
37. Barratt SL, Blythe T, Jarrett C, Ourradi K, Maher T, Welsh GI, et al. Differential expression of conventional and inhibitory VEGFA isoforms in normal and fibrotic fibroblasts–a potential role in IPF pathogenesis? *Thorax* 2013;68(Suppl2) http://dx.doi.org/10.1136/thoraxjnl-2013-204457.291. Unpublished paper.
38. Jenkins RG, Simpson JK, Saini G, Bentley JH, Russell AM, Braybrooke R, et al. Longitudinal change in collagen degradation biomarkers in idiopathic pulmonary fibrosis: an analysis from the prospective, multicentre PROFILE study. *Lancet Respir Med* 2015;3(6):462-72.
39. Varey AH, Rennel ES, Qiu Y, Bevan HS, Perrin RM, Raffy S, et al. VEGF 165 b, an antiangiogenic VEGF-A isoform, binds and inhibits bevacizumab treatment in experimental colorectal carcinoma: balance of pro- and antiangiogenic VEGF-A isoforms has implications for therapy. *Br J Cancer* 2008;98(8):1366-79.
40. Scotton CJ, Krupiczojc MA, Konigshoff M, Mercer PF, Lee YC, Kaminski N, et al. Increased local expression of coagulation factor X contributes to the fibrotic response in human and murine lung injury. *J Clin Invest* 2009;119(9):2550-63.
41. Qiu Y, Bevan H, Weeraperuma S, Wratting D, Murphy D, Neal CR, et al. Mammary alveolar development during lactation is inhibited by the endogenous antiangiogenic growth factor isoform, VEGF165b. *FASEB J* 2008;22(4):1104-12.
42. Gerber HP, Hillan KJ, Ryan AM, Kowalski J, Keller GA, Rangell L, et al. VEGF is required for growth and survival in neonatal mice. Development. 1999;126(6):1149-59.
43. Perl AK, Zhang L, Whitsett JA. Conditional expression of genes in the respiratory epithelium in transgenic mice: cautionary notes and toward building a better mouse trap.*Am J Respir Cell Mol Biol* 2009;40(1):1-3.
44. Scotton CJ, Hayes B, Alexander R, Datta A, Forty EJ, Mercer PF, et al. Ex vivo micro-computed tomography analysis of bleomycin-induced lung fibrosis for preclinical drug evaluation. *Eur Respir J* 2013;42(6):1633-45.
45. Meyer KC, Cardoni A, Xiang ZZ. Vascular endothelial growth factor in bronchoalveolar lavage from normal subjects and patients with diffuse parenchymal lung disease. *J Lab Clin Med* 2000;135(4):332-8.
46. Ando M, Miyazaki E, Ito T, Hiroshige S, Nureki S-i, Ueno T, et al. Significance of Serum Vascular Endothelial Growth Factor Level in Patients with Idiopathic Pulmonary Fibrosis. *Lung* 2010;188(3):247-52.
47. Cosgrove GP, Brown KK, Schiemann WP, Serls AE, Parr JE, Geraci MW, et al. Pigment epithelium-derived factor in idiopathic pulmonary fibrosis: a role in aberrant angiogenesis. *Am J Respir Crit Care Med* 2004;170(3):242-51.
48. Ye X, Abou-Rayyah Y, Bischoff J, Ritchie A, Sebire NJ, Watts P, et al. Altered ratios of pro- and anti-angiogenic VEGF-A variants and pericyte expression of DLL4 disrupt vascular maturation in infantile haemangioma. *J Pathol* 2016;239(2):139-51.

49. Carter JG, Gammons MV, Damodaran G, Churchill AJ, Harper SJ, Bates DO. The carboxyl terminus of VEGF-A is a potential target for anti-angiogenic therapy. *Angiogenesis* 2015;18(1):23-30.
50. Gammons MV, Fedorov O, Ivison D, Du C, Clark T, Hopkins C, et al. Topical antiangiogenic SRPK1 inhibitors reduce choroidal neovascularization in rodent models of exudative AMD. *Invest Ophthalmol Vis Sci* 2013;54(9):6052-62.
51. Nowak DG, Amin EM, Rennel ES, Hoareau-Aveilla C, Gammons M, Damodoran G, et al. Regulation of vascular endothelial growth factor (VEGF) splicing from pro-angiogenic to anti-angiogenic isoforms: a novel therapeutic strategy for angiogenesis. *J Biol Chem* 2010;285(8):5532-40.
52. Maurer B, Distler A, Suliman YA, Gay RE, Michel BA, Gay S, et al. Vascular endothelial growth factor aggravates fibrosis and vasculopathy in experimental models of systemic sclerosis. *Ann Rheum Dis* 2014;73(10):1880-7.
53. Hirigoyen D, Burgos PI, Mezzano V, Duran J, Barrientos M, Saez CG, et al. Inhibition of angiogenesis by platelets in systemic sclerosis patients. *Arthritis Res Ther* 2015;17:332.
54. Deng N, Sanchez CG, Lasky JA, Zhu D. Detecting splicing variants in idiopathic pulmonary fibrosis from non-differentially expressed genes. *PloS one* 2013;8(7):e68352.
55. Nance T, Smith KS, Anaya V, Richardson R, Ho L, Pala M, et al. Transcriptome analysis reveals differential splicing events in IPF lung tissue. *PloS one* 2014;9(3):e92111.
56. Carmeliet P, Moons L, Luttun A, Vincenti V, Compernolle V, De Mol M, et al. Synergism between vascular endothelial growth factor and placental growth factor contributes to angiogenesis and plasma extravasation in pathological conditions. Nat Med 2001;7(5):575-83.
57. Kamio K, Sato T, Liu X, Sugiura H, Togo S, Kobayashi T, et al. Prostacyclin analogs stimulate VEGF production from human lung fibroblasts in culture. *Am J Physiol Lung Cell Mol Physiol* 2008;294(6):L1226-32.
58. Jenkins G, Blanchard A, Borok Z, Bradding P, Ehrhardt C, Fisher A, et al. In search of the fibrotic epithelial cell: opportunities for a collaborative network. *Thorax* 2012;67(2):179-82.
59. Ashcroft T, Simpson JM, Timbrell V. Simple method of estimating severity of pulmonary fibrosis on a numerical scale. *J Clin Pathol* 1988;41(4):467-70.
60. Ebina M, Shimizukawa M, Shibata N, Kimura Y, Suzuki T, Endo M, et al. Heterogeneous increase in CD34-positive alveolar capillaries in idiopathic pulmonary fibrosis. *Am J Respir Crit Care Med* 2004;169(11):1203-8.

AJRCCM Articles in Press. Published on 29-June-2017 as 10.1164/rccm.201603-0568OC

Figure Legends

Figure 1: PanVEGF-A and VEGF-A $_{xxx}$b expression in the lungs of patients with IPF

a)PanVEGF-A RT-PCR of whole lung RNA extract using VEGF-A Exon2/3 For and 8b Rev primers (above) and Exon 7a For and 8b Rev primers (below) (n=5 normal lung and n=5 IPF lung). VEGF-A_{121}a, VEGF-A_{165}a and VEGF-A_{189}a isoforms were identified by RT-PCR and verified by direct sequencing (see E1). L indicates 50bp marker.

b)Quantitative RT-PCR (qRT-PCR) of panVEGF-A and VEGF-A_{xxx}b mRNA expression in whole lung tissue homogenates of normal (n=5) and IPF lung (n=5). No significant difference was detected in the expression of panVEGF-A or VEGF-A_{165}b (unpaired *t*-test) isoforms between normal and IPF lung samples.

c) PanVEGF-A and VEGF-A_{165}b ELISA data from lung whole tissue lysates in normal (n=5) and IPF (n=5) subjects. There was no significant difference in panVEGF-A expression (unpaired *t*-test with Welch's correction), but a significant increase in VEGF-A_{165}b expression in the IPF lung was observed (****$p<0.0001$, unpaired *t*-test). Data presented as means with SEM.

d) VEGF-A_{165}b ELISA data from plasma samples of IPF patients. VEGF-A_{165}b ELISA data from plasma samples of progressor (death or >10% decline in FVC at 12 months follow-up) and non-progressor IPF patients **(xx).** There was a significant difference in plasma levels of VEGF-A_{165}b in progressors (n=10) compared to non-progressors (n=15) (*$p<0.05$, unpaired *t*-test).

e) PanVEGF-A levels in bronchoalveolar fluid (BALF) of patients with IPF (n=15) compared to controls (n=13) using an antibody that does not discriminate between isoforms. Patient demographics were statistically comparable by unpaired *t*-test (E 2a) . PanVEGF-A BALF levels were significantly lower in the IPF group compared to control, **$p<0.01$, unpaired *t*-test with Welch's correction. Data presented as means with SEM: Mean panVEGF-A expression in control group 85.7pg/ml +/- 17.1, n=13 vs IPF 18.0pg/ml +/- 6.1. VEGF-A_{165}b expression was below the limit of detection in both IPF patients and controls (10pg/ml).

f) PanVEGF-A and VEGF-A_{165}b immunohistochemical staining: Intense staining of the alveolar epithelium was observed for both panVEGF-A and VEGF-A_{165}b in normal and IPF lungs (least and most fibrotic designated as in Ashcroft et al., and Ebina et al.(59, 60)) (block arrows). Additional sites of localisation included vessel walls (open arrow heads), fibroblasts (FFo indicates the fibrotic focus), lymphocytes and alveolar macrophages (AM). Isotype IgG shown as negative control. Scale bar =10μm, original magnification x100. Lower magnification images are shown in E2B.

Figure 2: VEGF-A receptor and co-receptor expression in the lungs of patients with IPF

a) Quantitative RT-PCR of VEGFR1,VEGFR2, NP1 and NP2 mRNA expression in whole lung RNA extracts of normal (n=5) and IPF lung (n=5). VEGFR1(*p<0.05, unpaired *t*-test) and NP1 (*p<0.05, unpaired *t*-test) mRNA expression was significantly up-regulated in the IPF lung. Data presented as mean fold change in expression (2^-ΔΔCT) with SEM, data analysis performed on ΔΔCT values.

b) VEGF-A receptor and co-receptor immunohistochemical staining: Intense staining of the alveolar epithelium was observed for VEGFR1, VEGFR2, NP1 and NP2 (block arrows) in both the normal and IPF lung. Additional sites of localisation included the vascular endothelium (open arrow heads), fibroblasts (FFo indicates the fibrotic focus), lymphocytes and alveolar macrophages (AM). Isotype IgG shown as negative control. Images taken at x40 magnification, scale bars 25μm. Additional higher magnification images are shown in E3B.

c) Expression of VEGFR1, VEGFR2, NP1 and NP2 in whole tissue lysates of normal (n=5) and IPF lung (n=5) by western blotting (above) with semi-quantitative densitometric analysis below. VEGFR1, VEGFR2, NP1 and NP2 were expressed in both the normal and IPF lung. VEGFR1(*p<0.05) was significantly down-regulated in the IPF lung (unpaired *t*-test, data presented as mean densitometry score with SEM).

AJRCCM Articles in Press. Published on 29-June-2017 as 10.1164/rccm.201603-0568OC

Figure 3: VEGFR and VEGF-A isoform expression in NF and FF

a)Expression of VEGFR1, VEGFR2, NP1 and NP2 in NF and FF by western blotting with semi-quantitative densitometric analysis. Using glomerular endothelial cells as a positive control (Ctrl), bands were observed by western blotting that were consistent with the expression of VEGFR1, NP1 and NP2 in both NF and FF. Mature VEGFR2 protein was not expressed by NF or FF fibroblasts (data not shown). Semi-quantification of expression by densitometry demonstrated a significant reduction in the expression of VEGFR1 (*$p<0.05$) and NP2 (*$p<0.05$) in un-stimulated FF cultures compared to NF (data presented as means with SEM, NF: n=4, FF: n=4, n=3 or n=4 shown, unpaired *t*-test).

b)Western blot of phosphorylated MEK1/2 and phosphorylated p42/p44 MAPK (mitogen-activated protein kinase) expression in response to 24 hours of stimulation with VEGF-A_{165}a (20ng/ml) or VEGF-A_{165}b (20ng/ml). In the absence of mature VEGFR2 expression in NF and FF, the activation of known VEGF-A signaling pathways was explored. Stimulation of NF and FF led to the increased phosphorylation of MEK1/2 and p42/p44 in response to treatment of cells with VEGF-A_{165}a or VEGF-A_{165}b. For densitometric analysis see Fig. E4.

c) Western blot of panVEGF-A and VEGF-A_{165}b expression in NF and FF cell lysates with semi-quantitative densitometric analysis (data presented as means with SEM). Recombinant proteins were used as positive controls to highlight the specificity of the VEGF-A_{165}b antibody in detecting VEGF-A_{165}b proteins. The dotted line in the lower blot indicates where the blot has been manually cut and components images separately. VEGF-A_{165}b proteins were significantly up-regulated in FF cell lysates compared to NF (n=3, *$p<0.05$, unpaired *t*-test). No significant difference in panVEGF-A isoform expression was shown (n=3, unpaired *t*-test).

d) Quantification of protein expression of panVEGF-A and VEGF-A_{165}b expression in NF and FF cell lysates. By ELISA there was no significant difference in the expression of panVEGF-A or VEGF-A_{165}b in NF or FF cell lysates (n=6 performed in duplicate cell lysates of different passage, unpaired *t*-test). In the conditioned medium extracted from these cultures panVEGF-A expression was significantly up-regulated in the FF supernatants (n=6, *$p<0.05$, unpaired *t*-test)-see Fig E7. VEGF-A_{165}b expression in these same cell supernatant samples was below the limit of detection of the ELISA (10*p*g/ml).

e) Cell immunofluorescence of panVEGF-A and VEGF-A_{165}b expression in NF and FF. Comparable patterns were observed for NF and FF, with cytoplasmic, and perinuclear expression of panVEGF-A and cytoplasmic expression of VEGF-A_{165}b. Images taken at x40 magnification with scale bar indicating 25μm. Primary antibody shown in green with an overlay image of the primary antibody, phalloidin (red) for F-actin and DAPI (blue) for nuclear staining. Isotype IgG controls and separate phalloidin and DAPI images shown in supplementary data (E8).

Figure 4: Functional response of NF and FF to recombinant VEGF-A proteins

a)The effect of VEGF-A on the expression of fibronectin (FN) by NF and FF in response to 24 hours of stimulation with VEGF-A_{165}a (20ng/ml) or VEGF-A_{165}b (20ng/ml) as measured by western blotting (above) with densitometry analysis (below). A significant increase in the expression of FN in response to VEGF-A_{165}a stimulation in both NF(**$p<0.01$ with 10ng/ml and 20ng/ml) and FF ($^{+++}p<0.001$ at 20ng/ml, n=3) was observed. There was no significant effect of VEGF-A_{165}b on the expression of FN in neither NF or FF.

b)The combined effect of VEGF-A_{165}a and VEGF-A_{165}b on the expression of FN in NF and FF as measured by western blotting (above) and densitometry (below). Used in isolation, VEGF-A_{165}a (20ng/ml) was shown to increase FN expression in NF ($^{X}p<0.05$) and FF ($^{XX}p<0.01$), whilst VEGF-A_{165}b had no significant effect, as shown in the previous experiments. VEGF-A_{165}b inhibited the VEGF-A_{165}a-induced increase in FN expression in both NF (*$p<0.05$ at 40ng/ml of VEGF-A_{165}b) and FF ($^{+++}p<0.001$ at 10, 20 and 40ng/ml of VEGF-A_{165}b) with FF appearing to be more susceptible to this effect (n=3). Data presented as means with SEM.

c) The effect of VEGF-A on the expression of collagen by NF and FF in response to 24 hours of stimulation with VEGF-A_{165}a or VEGF-A_{165}b as measured by HPLC.. In the presence of both isoforms, VEGF-A_{165}b inhibited collagen production in NF but not FF (*$p<0.05$, **$p<0.01$) (NF and FF n=3). Data presented as means with SEM.

d) The effect of VEGF-A recombinant proteins on the proliferation of NF and FF: A significant increase in FF cell number was observed in response to 20ng/ml VEGF-A_{165}a compared to SFM ($^{X}p<0.05$). VEGF-A_{165}a-induced proliferation was inhibited by the concomitant addition of 20ng/ml VEGF-A_{165}b ($^{+++}p<0.001$) or 10ng/ml sFlt ($^{+++}p<0.001$). VEGF-A_{165}a had no statistically significant effect on NF cell proliferation compared to SFM, but concomitant treatment of NF with 20ng/ml VEGF-A_{165}a and 20ng/ml VEGF-A_{165}b (*$p<0.05$) or sFlt (*$p<0.05$) inhibited cell proliferation compared to 20ng/ml VEGF-A_{165}a alone (*$p<0.05$) (NF and FF n=5). Data presented as means with SEM.

e) The effect of VEGF-A recombinant proteins on NF and FF wound healing. Image analysis performed using Image J. VEGF-A_{165}a and VEGF-A_{165}b significantly increased the migration of NF at 48 hours (*$p<0.05$). This effect was blocked by the concomitant treatment of VEGF-A_{165}a and VEGF-A_{165}b. Recombinant VEGF-A proteins had no significant effect on the migration of FF. Statistical analysis: ANOVA with post-hoc Holm's Sidak multiple comparisons analysis used throughout (n=4). Representative images shown in E9.

AJRCCM Articles in Press. Published on 29-June-2017 as 10.1164/rccm.201603-0568OC

Figure 5: The effect of post-natal deletion of VEGF-A from ATII cells on the development of pulmonary fibrosis

a) GFP-eporter mice ($ROSA^{mT/mG}$) were crossed with $SPC^{+/-}TC^{+/-}LoxP^{+/-}$ TG mice (STCL) to determine the period of doxycycline induction required to activate the Cre-recombinase and to identify the tissue specificity of Cre-recombinase activity following doxycycline induction. The reporter mice possess LoxP sites on either side of a membrane-targeted tdTomato (mT) cassette and express red fluorescence in all tissues. In the presence of Cre recombinase, the mT cassette is deleted allowing expression of the membrane-targeted EGFP (mG) cassette located just downstream. The *in vivo* imaging system (IVIS) demonstrated evidence of GFP fluorescence in the GFP-STCL mouse following 10 weeks of doxycycline induction, absent at 4 weeks of induction and in WT mice. Direct visualisation of the lungs of induced mice (at 12 and 14 weeks of doxycycline treatment), demonstrated GFP fluorescence in ATII cells with an absence of GFP fluorescence in the bronchial epithelium (14 weeks induction image, arrows). Images taken at x40 magnification, scale bar 25μm, n=3. GFP fluorescence was absent in the kidneys and liver (see supplementary data E10). Using a murine VEGF-A RNA probe, *in situ* hybridisation demonstrated a reduction in ATII cell staining (reduction in blue/black signal) in induced-TG mice compared to induced-WT mice (arrows). Pink staining represents nuclear fast red counterstain (n=3, images taken at x100 magnification, scale bar = 10μm). PanVEGF-A mRNA expression was significantly reduced in whole tissue RNA extracts from TG mice compared to WT mice (n=6, **$p<0.01$, unpaired *t*-test, data presented as means with SEM). Consistent with these findings, immunohistochemical staining for panVEGF-A also showed a reduction in ATII cell staining in induced-TG mice compared to induced-WT mice (n=3, images taken at x100 magnification, scale bar = 10μm).

b) Post-natal deletion of VEGF-A from ATII cells ameliorates the development of BLM-induced pulmonary fibrosis. Masson's Trichrome staining of mouse lung sections, with lung fibrosis score and quantitative RT-PCR of FN and pro-collagen-1α mRNA levels above (below). As demonstrated by Masson's Trichrome staining, administration of BLM to both WT (g-i) and non-induced STCLL (j-l) mice resulted in extensive pulmonary fibrosis. This effect was ameliorated in BLM-treated doxycycline-induced STCLL mice (m-o). Images originally x10 magnification, scale bar = 100μm, n=5 or 6, n=3 shown). The lung fibrosis score of BLM-treated, doxycycline-induced STCLL mice was significantly reduced compared to BLM-treated controls (induced-WT mice **$p<0.01$ and non-induced STCLL mice **$p<0.01$, n = 5).The expression of FN and pro-collagen-1α mRNA was significantly up-regulated in the lungs of BLM-treated, doxycycline-induced WT mice compared to saline treated controls (****$p<0.001$, n=5 or 6 analysed). FN and pro-collagen-1α expression was significantly up-regulated in BLM-treated, doxycycline-induced TG mice compared to TG saline controls (*$p<0.05$, **$p<0.01$, n=5). Furthermore, FN mRNA levels were significantly reduced in BLM-treated TG mice compared to BLM-treated WT mice (*$p<0.05$, n=5), with a trend towards a reduction in pro-collagen-1α levels in these same mice ($p=0.08$, n=5). Statistical analysis: ANOVA with Holm's Sidak multiple comparisons test used throughout.

Figure 6: The effect of VEGF-A_{165}b on the development of pulmonary fibrosis.

a) Lung phenotype of the MMTV-VEGF-A_{165}b TG mouse: Immunohistochemical staining for VEGF-A_{165}b in the lung of TG mice with quantification of VEGF-A_{165}b expression by ELISA, in whole tissue lysates and BALF fluid. VEGF-A_{165}b expression was increased in the ATII cells of the TG mouse lung ((d +f) indicated by arrows) compared to the WT lung (c+e). Isotype IgG staining was used as a negative control (a+b). Images taken at x100 magnification, scale bars 10μm, (n=3, n=1 shown). VEGF-A_{165}b expression was significantly up-regulated in whole tissue lysates of TG mice compared to WT mice (*$p<0.05$, unpaired *t*-test with Welch's correction, n=4). The expression of VEGF-A_{165}b was below the limit of detection of the ELISA in all BALF samples of WT mice but present in detectable levels in all BALF samples of TG mice. There was no statistical difference between these groups ($p=0.055$, unpaired *t*-test with Welch's correction, n=4).

b) Over-expression of VEGF-A_{165}b in ATII cells ameliorates the development of BLM- induced pulmonary fibrosis. Representative images of Masson's Trichrome staining with lung fibrosis score and quantitative RT-PCR of FN and pro-collagen-1α mRNA levels (below). Masson's Trichrome staining of mouse lung sections, 21 days following OP instillation of BLM to MMTV-VEGF-A_{165}b TG mice (j-l) or littermate controls (g-i). The development of BLM-induced pulmonary fibrosis was ameliorated in TG mice. Saline controls demonstrated in (a-f), (n=6 per group, n = 3 shown). Scale bar 100μm, original magnification x10. The lung fibrosis score of BLM-treated TG mice was significantly lower than BLM-treated WT mice (***$p<0.001$, n=6 per group). FN mRNA was significantly up-regulated in the lungs of WT BLM-treated mice compared to WT-saline treated controls (**$p<0.01$, n=6 analysed) and in TG BLM-treated mice compared to TG saline-treated controls (*$p<0.05$) (n=6). There was no statistical difference between BLM-treated WT and TG mice ($p=0.09$, n=6). In contrast, pro-collagen-1α mRNA levels were significantly reduced in BLM-treated TG mice compared to BLM-treated WT littermates *$p<0.05$, n=6). Data presented as means with SEM. Statistical analysis: ANOVA with Holm's Sidak multiple comparisons test used throughout.

c) IP instillation of rhVEGF-A_{165}b ameliorates the development of pulmonary fibrosis. Masson's Trichrome staining of lung sections with lung fibrosis score and quantitative RT-PCR of FN and pro-collagen-1α mRNA levels (below). Representative images of Masson's Trichrome staining of mouse lung sections, 21 days following OP instillation of Bleomycin with or without additional IP rhVEGF-A_{165}b instillation: (a-c) OP Saline control (no differences between Early IP VEGF-A_{165}b (EV) or late IP VEGF-A_{165}b (LV) plus saline), (d-f) OP Bleomycin with saline IP (g-i) Early IP VEGF-A_{165}b treatment with subsequent Bleomycin OP instillation (j-l) Bleomycin OP with subsequent late IP VEGF-A_{165}b instillation. Early and late rhVEGF-A_{165}b instillation ameliorated the development of lung fibrosis (n=6 per group, n=3 shown). Scale bar 100μm, original magnification x10. By qRT-PCR FN and pro-collagen-1α mRNA was significantly up-regulated in the lungs of BLM-treated mice compared to saline-treated controls (*$p<0.05$, **$p<0.01$, n=5). In contrast, FN and pro-collagen-1α expression in mice treated with either early (EV) or late (LV) rhVEGF-A_{165}b and BLM was not significantly different to saline control (n=6). The lung fibrosis score in both early (EV, **$p<0.01$) and late (LV, *$p<0.05$) IP rhVEGF-A_{165}b treatment groups was significantly reduced compared to BLM OP-Saline IP treated mice, n=5 or 6 per group, data presented as means with SEM. Statistical analysis: ANOVA with Holm's Sidak multiple comparisons test used throughout.

AJRCCM Articles in Press. Published on 29-June-2017 as 10.1164/rccm.201603-0568OC

Figure 1

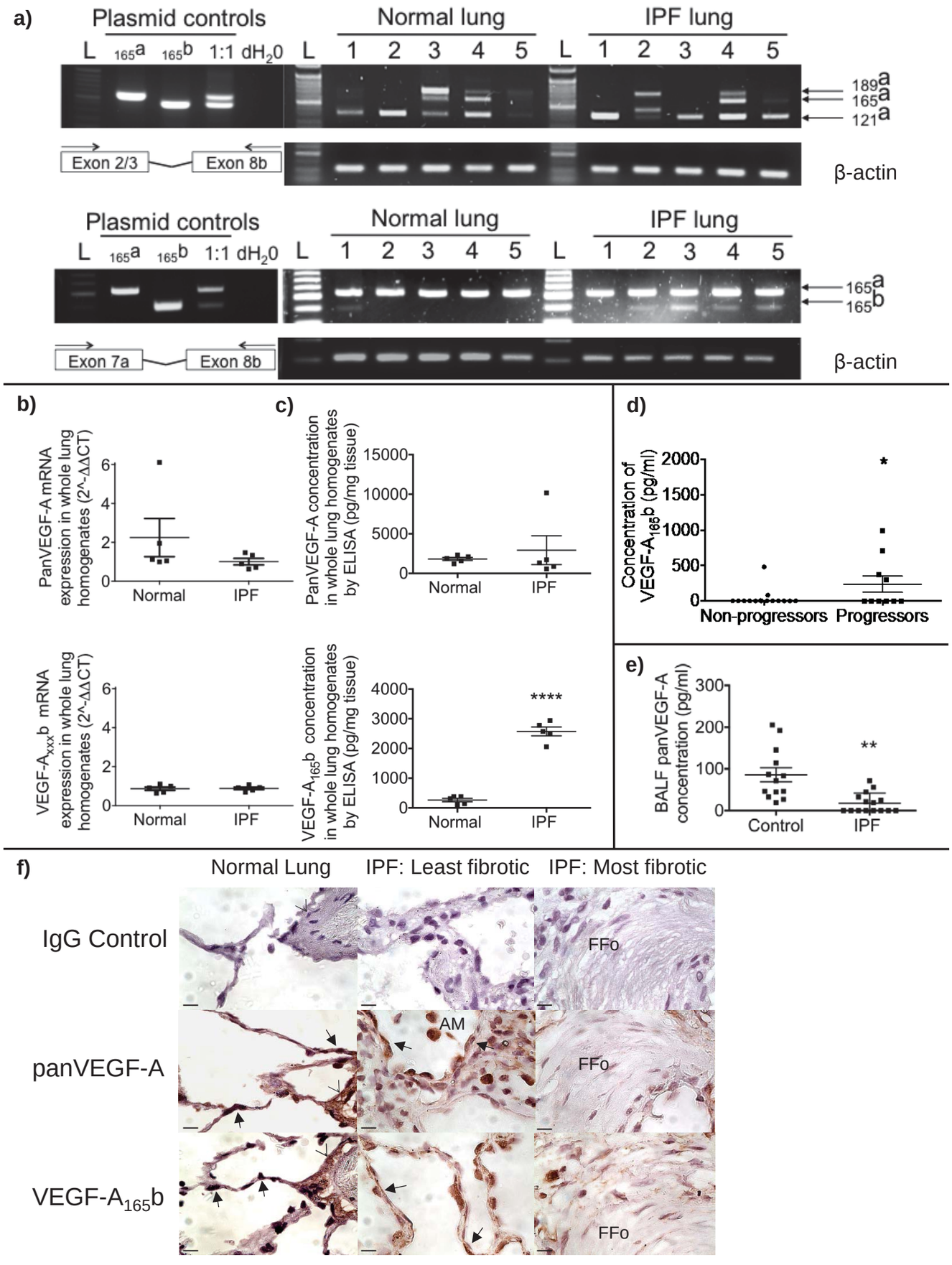

Figure 2

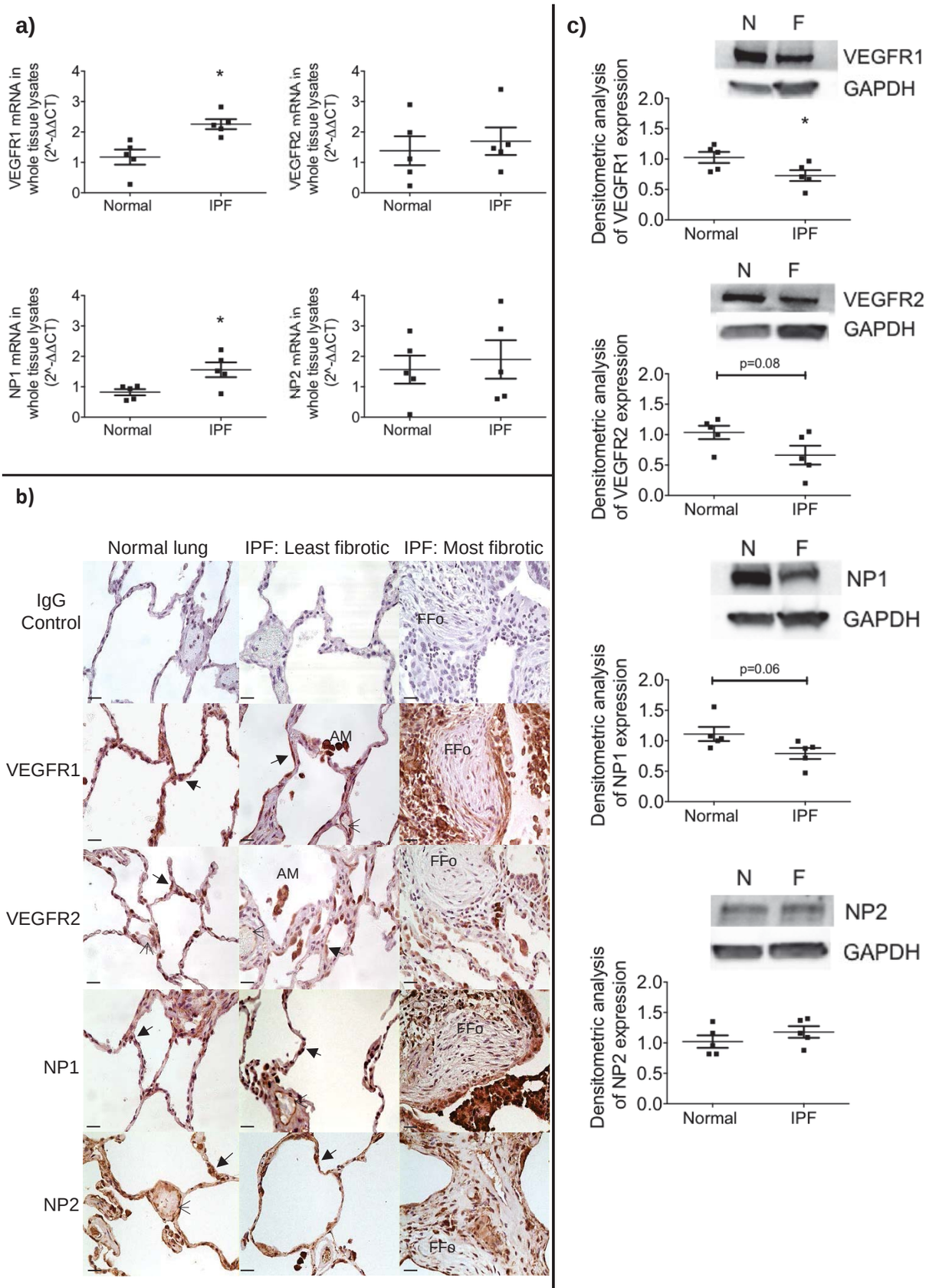

AJRCCM Articles in Press. Published on 29-June-2017 as 10.1164/rccm.201603-0568OC

Figure 3

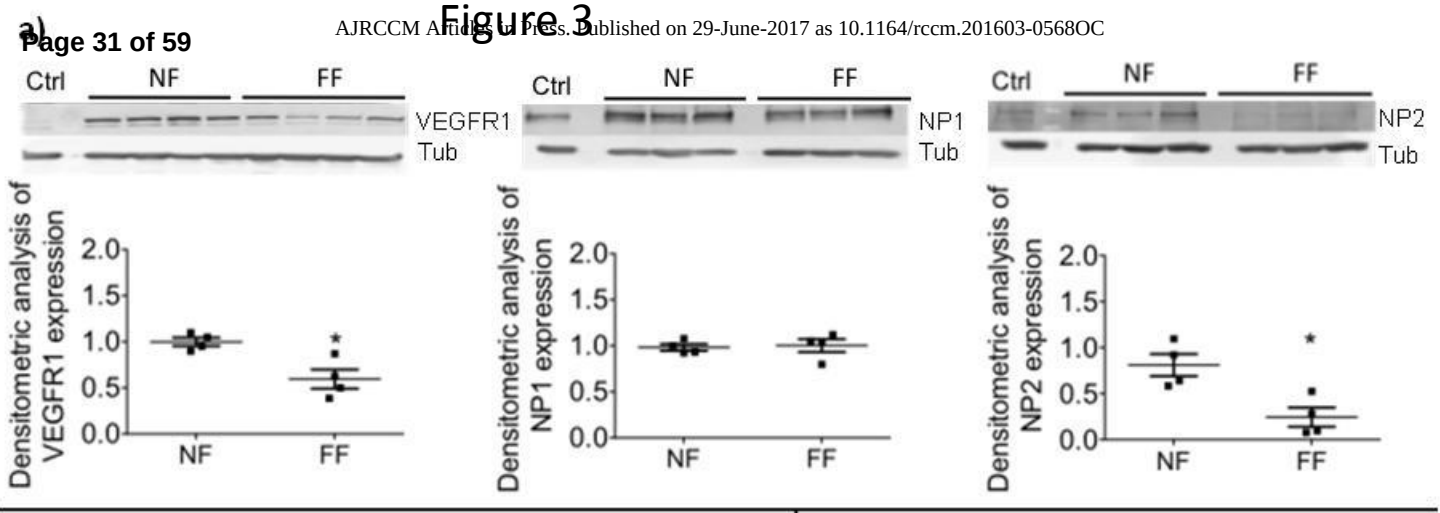

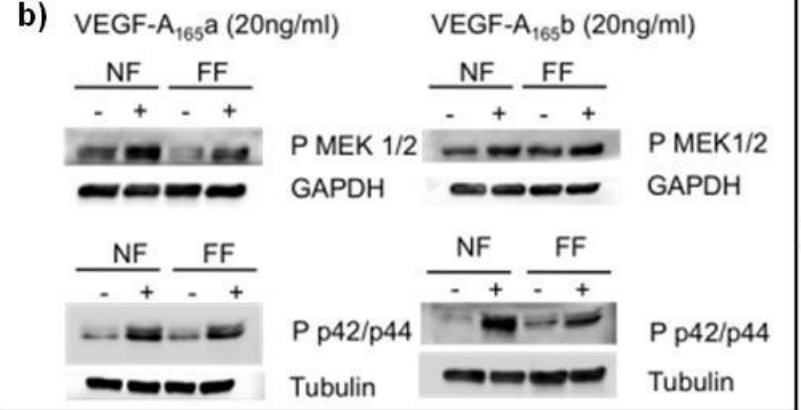

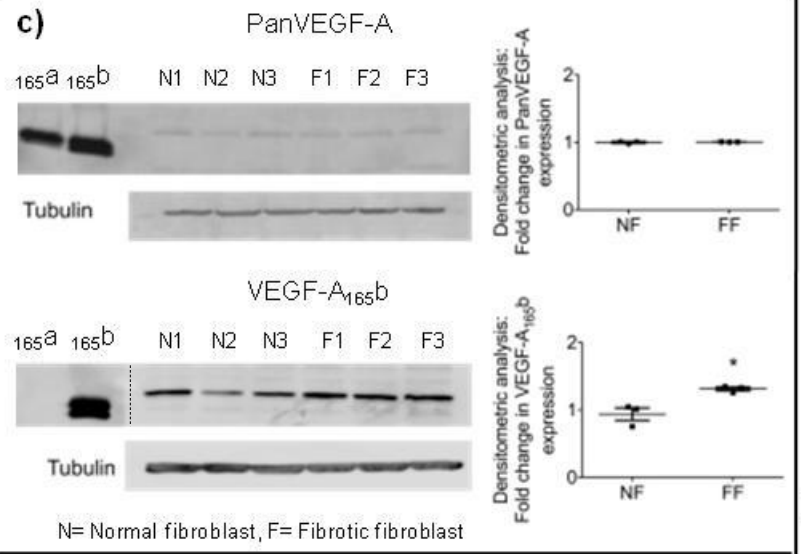

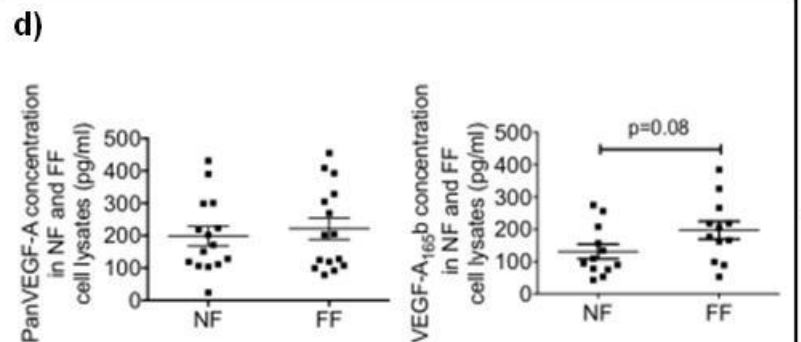

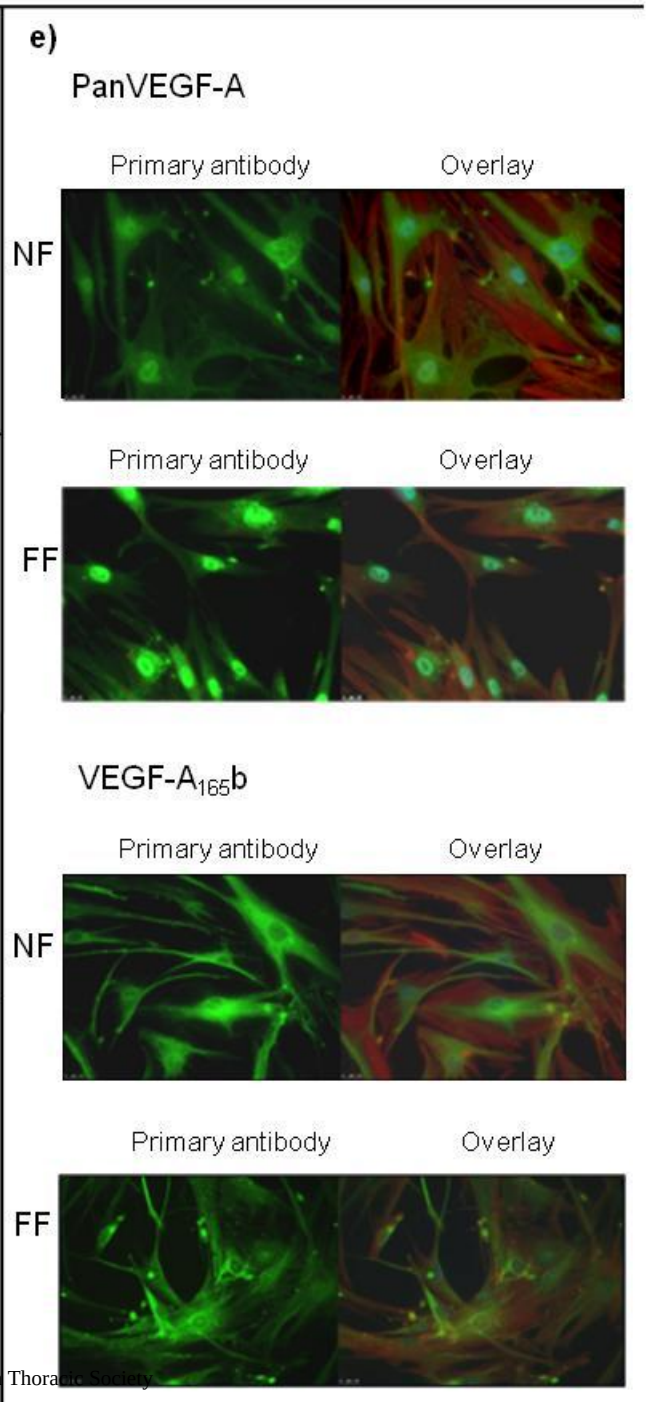

Figure 4

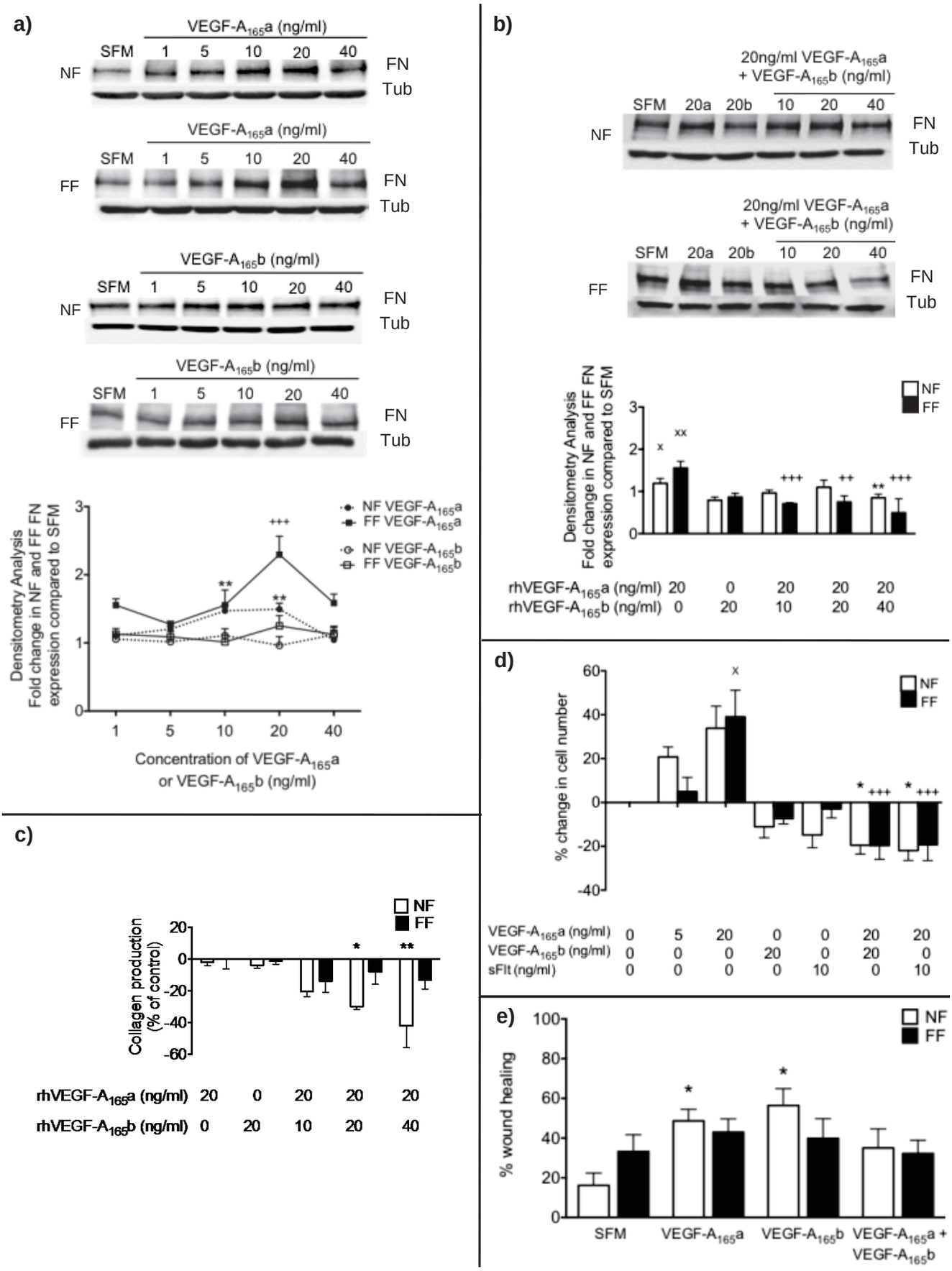

AJRCCM Articles in Press. Published on 29-June-2017 as 10.1164/rccm.201603-0568OC

Figure 5

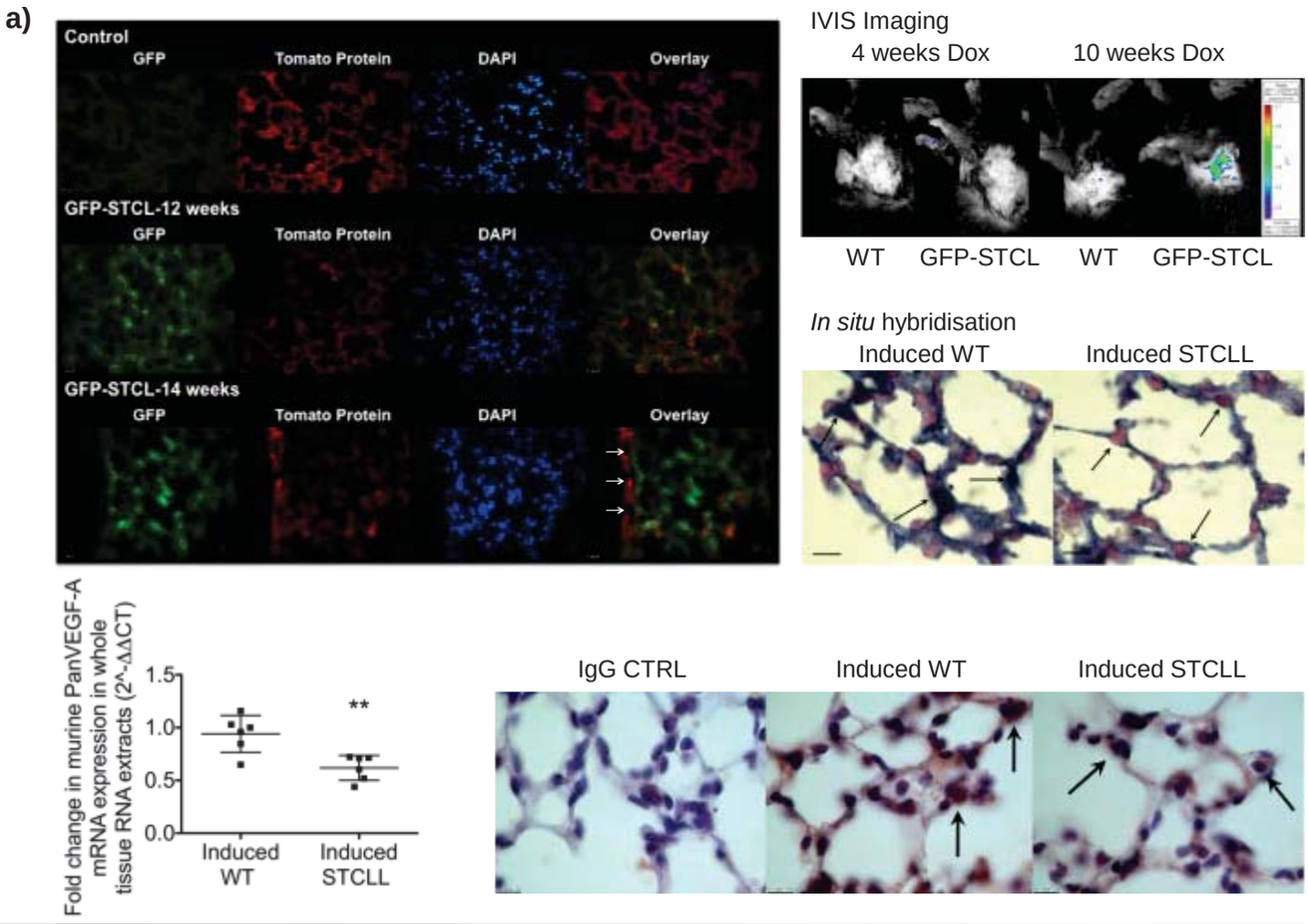

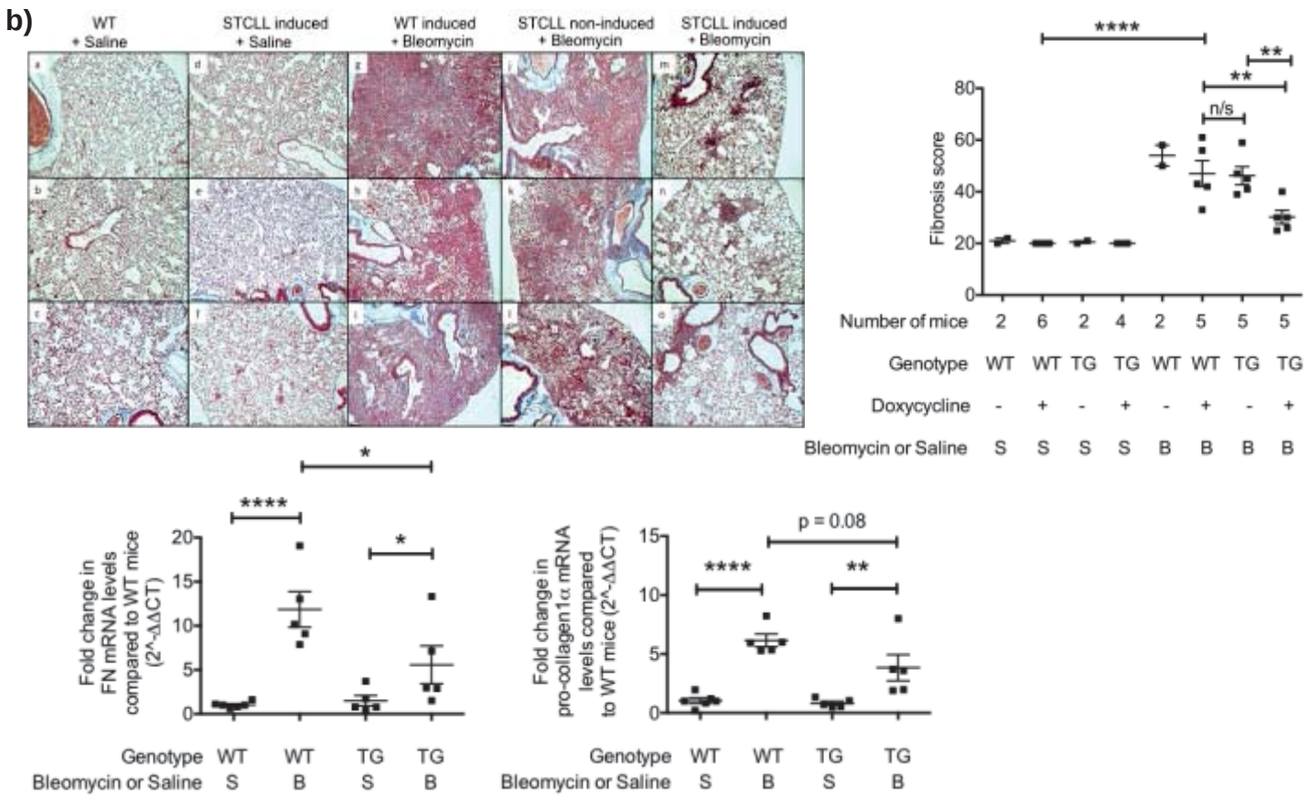

Figure 6

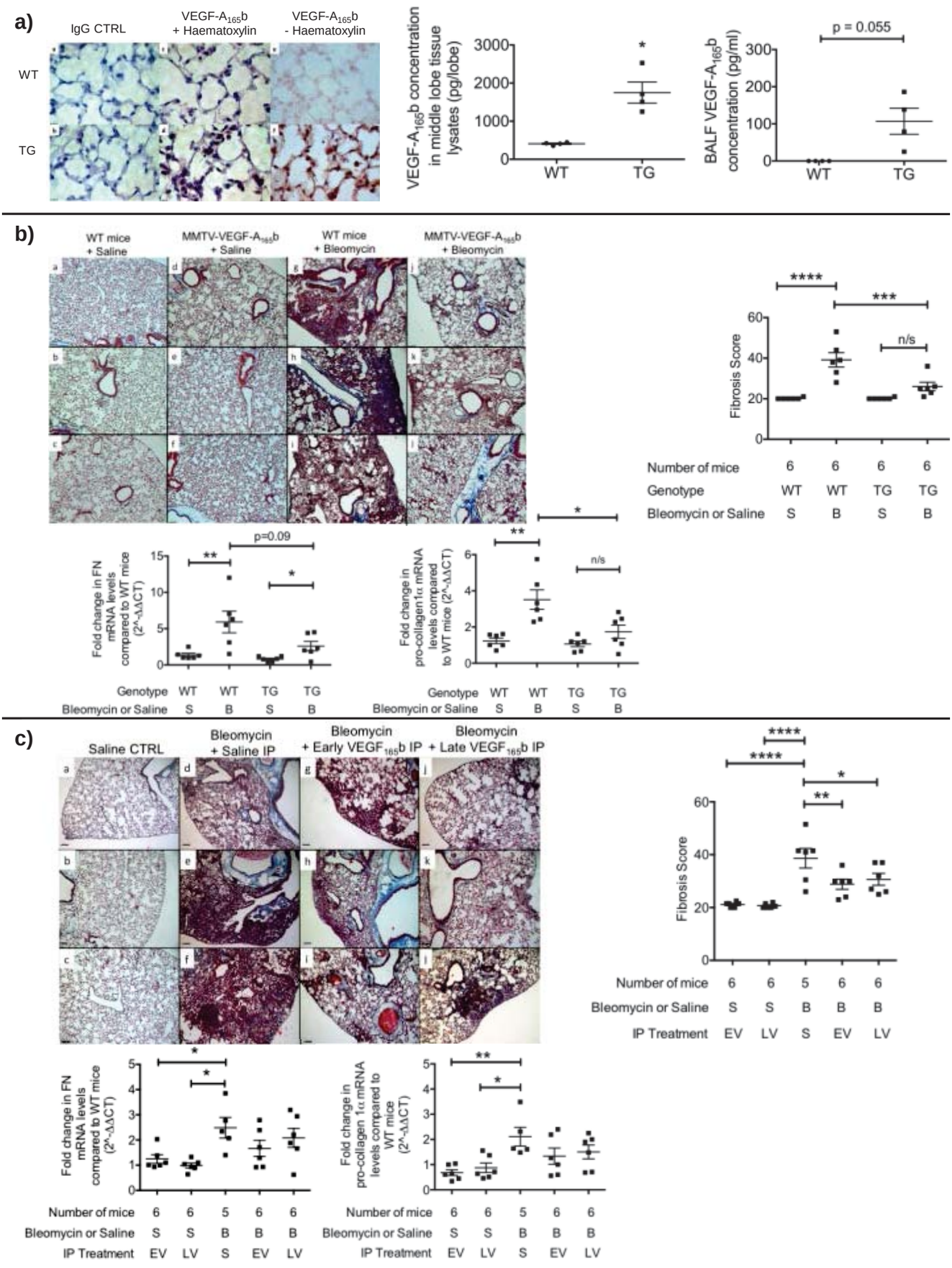

AJRCCM Articles in Press. Published on 29-June-2017 as 10.1164/rccm.201603-0568OC

ON-LINE supplement.

Differential expression of VEGF-A_{xxx} isoforms is critical for development of Pulmonary Fibrosis

Authors: S.L.Barratt[1], T.Blythe[1], C.Jarrett[1], K.Ourradi[1], G.Shelley-Fraser[2], M.J.Day[3], Y.Qiu[4], S.Harper[4], T.M.Maher[5], S.Oltean[6], T.J.Hames[7], C.J.Scotton[7], G.I.Welsh[4], D.O.Bates[8], A.B.Millar[1*]

Materials and Methods

Human tissue collection

Anonymised human lung biopsies were donated from patients undergoing clinically indicated open or VATS thoracoscopy. Tissue surplus to diagnostic requirements with a histopathological appearance of either normal alveolar tissue or a pattern of UIP (for patients with IPF) was accepted. The institutional review boards of both North Bristol and United Bristol Healthcare Trusts granted ethical approval. Written informed consent was obtained from each patient. Additional IPF lung samples were donated from the Lung Tissue Research Consortium (LTRC), USA.

Bronchoscopy and Bronchoalveolar lavage (BAL) were performed according to standard protocols. These were not performed on the subjects from whom the lung tissues were obtained. The BAL fluid (BALF) was immediately spun at 500*g* for 5 min and supernatant was collected and stored at −80°C until required.

Plasma samples were donated by Toby Maher, Royal Brompton hospital. These were obtained as additional samples to the PROFILE study and classified as stable vs progressors as described previously (**ref**: E1)

Primary lung fibroblast culture

Primary lung fibroblasts were explanted from whole lung tissue biopsies using established techniques and cell cultures maintained under standard growth conditions (37°C in a humidified atmosphere consisting of 95% air and 5% CO_2) in DMEM-F12 media (Gibco) supplemented with 1% Fungizone (Gibco), 1% penicillin/streptomycin (Sigma, P43330) and 10% Heat inactivated Newborn Calf Serum (Gibco).

Additional IPF fibroblast cultures were donated (Toby Maher, Royal Brompton Hospital). Normal and IPF fibroblast cultures (ATCC, American Type Culture Collection) were also purchased.

Stimulation of NF and FF with rhVEGF-A_{165}a or rhVEGF-A_{165}b:

For all experiments cells were grown to 80% confluence in T25 Corning flasks, prior to induction of cell quiescence in SFM for 24 hours.

To determine NF and FF fibronectin expression, confluent, growth arrested cells were treated with serial concentrations of rhVEGF-A_{165}a (Cell Signaling) or rhVEGF-A_{165}b (R&D) alone and in combination for 24 hours. mRNA and protein were isolated for analysis by qRT-PCR (n=4) and western blotting (n=3), respectively.

To determine the signalling characteristics of pulmonary fibroblasts in response to VEGF-A recombinant proteins, cells were then incubated for 10 minutes with either a) SFM,

b) rhVEGF-A_{165}a 20ng/ml or c) rhVEGF-A_{165}b 20ng/ml, prior to lysis in RIPA buffer for protein analysis.

RT-PCR for detection of VEGF-A isoforms

Total RNA was isolated from human lung tissue or fibroblast lysates using the Quick RNA™ mini prep kit (R1054, Zymo Research), as per manufacturer's instructions to prevent gDNA contamination. RNA, 0.4-1µg, was reverse transcribed into cDNA using the Taqman High Capacity RNA-to-cDNA kit (Applied Biosystems). cDNA was subjected to PCR with one of two primer sets: Forward primer 5'-CGA AGT GGT GAA GTT CAT GGAT G-3', spanning exon 2/3 and reverse primer 5'-TTCTGTATCAGTCTTTCCTGGTGA-3', located within the 3'UTR of exon 8b or Forward primer: 5'-GTTTGTACAAGATCCGCAGACGT-3' located within exon 7a and the same reverse primer 5'-TTCTGTATCAGTCTTTCCTGGTGA-3', located at the 3'UTR of exon 8b. VEGF-A_{165}a and VEGF-A_{165}b plasmid templates (pcDNA3-VEGF-A_{165}a or pcDNA3-VEGF-A_{165}b) (1µl of 0.1ng/µl) were used as positive controls. An additional reaction was carried out with a 1:1 mix of each template (0.5µl of 0.1ng/µl of each template) to demonstrate that the RT-PCR reaction could amplify both templates if present. Samples were run in 1xTAE buffer and then bands excised for direct sequencing.

RT-PCR was also used to demonstrate human VEGF-A_{165}b expression in the TG MMTV-$_{165}$b mouse lung, the human panVEGF-A primers: exon 7a For and 8b Rev were used, in addition to primer sets that specifically detected the presence of the MMTV-$VEGF_{165}$b transgene: For (exon 7): 5'- ACA AGA TCC GCA GAC GTG TA-3', Rev (Poly-A tail): 5'- ACA GAT GGC TGG CAA CTA-3'.

Quantitative RT-PCR

Total RNA was isolated and reverse transcribed into cDNA as described above. Individual qRT-PCR reaction mixes were made according to manufacturer recommendations (2x SensiFAST SYBR Hi-ROX (Bioline)).

Human and murine primer sets used are detailed in Supplementary Tables 1 and 2, respectively. Using a qPCR method previously published by Varey et al (ref:E2), the expression of human VEGF-A_{xxx}a and VEGF-A_{xxx}b isoforms were also quantified. Primer sequences available upon request.

The standard cycling regime used consisted of: 95^{o}C for an initial 2 mins, followed by thermal cycles of 95^{o}C for 5 secs and 60^{o}C for 30 secs, for 50 cycles for identification of VEGF-A isoforms and 40 cycles for all other products. Minus reverse transcriptase and non-template control reactions were additionally performed as negative controls. The expression level of each gene was normalised to β-actin expression, for human samples or HPRT for murine samples. The specificity of the PCR-products was confirmed by melt-curve analysis.

Fluorescence data from each sample were analysed with the $2^{-\Delta\Delta Ct}$ method, where ΔΔCt = (Ct GI unknown sample – Ct Actin unknown sample) – (Ct GI calibrator sample – Ct Actin calibrator sample), where GI is the gene of interest. Statistical analyses were performed on ΔΔCT values.*Cell Immunofluorescence*

Cells were grown to 80% confluence on sterile glass coverslips. Cells were fixed for 10 minutes in 2% paraformaldehyde in PBS. Cells were permeabilised in with 0.3% TritonX-100 (Fischer Scientific) and blocked in a 5% HI NCS (Gibco), 2% BSA (Fischer Scientific, BPE) and 0.1% Tween x20 (Sigma) in PBS for 30 minutes. Cells were incubated with the

AJRCCM Articles in Press. Published on 29-June-2017 as 10.1164/rccm.201603-0568OC

primary antibody of interest, overnight at 4˚C. Primary antibodies were prepared at a concentration of 1 in 50 in blocking solution: VEGFR1(AbCam), VEGFR2 (Cell Signaling), NP1 (AbCam), NP2 (Santa Cruz), panVEGF-A (Santa Cruz) and VEGF-A_{165}b (AbCam).

The following day, cells were incubated with the appropriate secondary antibody for one hour: Invitrogen Alexa Fluor 488 Goat anti-mouse IgG or Invitrogen Alexa Fluor Goat anti-rabbit IgG at a concentration of 1 in 200 in blocking solution. DAPI (4',6-diamidino-2-phenylindole) (Invitrogen) and Phalloidin 568 (Invitrogen) were used as counterstains for nuclear and F-actin, respectively. Mounted coverslips were examined using a Leitz DMRB fluorescent microscope (Leica, Solms, Germany) and images captured (Leica EL6000 digital camera and Leica Application Suite Advanced Fluorescent (LASAF) software). Comparison of overlaid images enabled identification of cellular expression.

Western-Blot Analysis

Cell lysates were prepared from fibroblast cultures (Passage (P) 2-7), using RIPA (radio-immunoprecipitation) extraction buffer (Sigma, R0278), containing 1:100 protease inhibitor cocktail (Sigma) and 1:100 phosphatase inhibitors (Sigma). Whole lung tissue lysates were prepared in Triton-X100 containing protease and phosphatase inhibitors. Cell lysate protein was quantified using a BCA (bicinchoninic acid) protein assay kit (Fischer Scientific) as per the manufacturer's guidelines.

Protein (30-45µg) was loaded into 8-12% acrylamide gels and transferred to PolyVinylidine DiFluoride (PVDF, Millipore 0.45µm) membrane, incubated in blocking buffer (5% non-fat dried milk in 1 X TBST) for one hour and then in primary antibody overnight. Primary antibodies: VEGFR1 (Abcam), VEGFR2 (Cell Signaling), NP1 (Abcam), NP2 (Santa Cruz), panVEGF-A (Santa Cruz) and VEGF-A_{165}b: donated by D.O.Bates, Fibronectin: (BD Transduction labs), Phospho MEK1/2 (Cell Signaling), Phospho p42/p44 (Cell Signaling), Lamin (Cell Signaling), β-Actin (Sigma), Tubulin (Sigma), GAPDH (Millipore).

Membranes were then incubated with a HRP-conjugated secondary antibody (donkey anti-rabbit or sheep anti-mouse GE Healthcare) in blocking buffer for 1 hour prior to visualisation by means of luminol-enhanced chemiluminescence (SuperSignal, West Femto, 34096, Thermo Scientific) and imaged with a UVP ChemiDoc-It imaging system (UVP, California, USA) and Visionworks LS software. Equal protein loading per lane was confirmed using β-actin, GAPDH or tubulin controls.

Lysates from conditionally immortalised glomerular endothelial cells (P20) were used as a positive control for VEGF receptor expression, whilst recombinant rhVEGF-A_{165}a (Cell Signaling) and rhVEGF-a_{165}b (R&D) proteins provided positive controls for VEGF-A isoform expression. Semi-quantification of protein expression was undertaken by densitometry using Image-J software.

Immunohistochemistry

Slides were de-waxed in xylene prior to rehydration of tissue in decreasing concentrations of ethanol, then rinsed in dH_2O prior to antigen retrieval in sodium citrate buffer (10mM Sodium citrate in 0.05% Tween 20, pH6). For the localisation of NP2 in human tissues a TRIS-EDTA (10mM Tris Base, 1mM EDTA, 0.05% Tween, pH9.0) antigen retrieval buffer was used. Endogenous peroxidases were blocked with 30% hydrogen peroxide (H_2O_2) (Sigma) in Methanol (Fisher Scientific) and dH_2O, washed, then blocked with 2.5% normal horse serum (NHS)(provided in Vector IMMPRESS reagent kits). Sections

were incubated with primary antibody (concentration of 1:100 in 2.5% NHS block) or appropriate IgG control.

Slides were washed in TBS before addition of secondary antibody (Vector IMMPRESS reagent kit (peroxidase) anti-mouse IgG (MP7402) or anti-rabbit (MP7401), washed and substrate (Vector NovaRED substrate kit for peroxidase) added until a red colour was visible and |counterstained with Haematoxylin (Vector).

For dual stained sections: Following completion of the substrate step, sections were blocked in 2.5% NHS. Slides were incubated in the second primary antibody (E-Cadherin – diluted 1:50 in 1% BSA in PBS) then washed and the secondary antibody applied (anti-mouse IgG polymer HRP – Vector) as per manufacturer instructions. The SG Peroxidase substrate kit was applied (Vector) then rinsed with dH_2O.

Slides were dehydrated and then cleared in xylene (4 mins) before mounting and subsequent imaging (Leitz DMRB microscope (Leica, Solms, Germany) using the Leica EL6000 digital camera and Leica Application Suite Advanced Fluorescent (LASAF) software).

ELISA of PanVEGF-A and VEGF-A_{165}b

Protein was isolated from fibroblast cell cultures using RIPA buffer (Sigma) and protein quantified by BCA analysis (Thermo Scientific, Pierce). Human lung tissue was initially weighed (wet weight) and protein isolated using mechanical homogenisation in 1% Triton extraction buffer containing protease and phosphatase inhibitors. Commercially available ELISA kits were used to quantify panVEGF-A (R&D systems) and VEGF-A_{165}b levels (R&D systems) in BALF, human lung tissue, fibroblast cell lysates, cell supernatants and plasma according to manufacturer's instructions.

Cell Proliferation assay

Fibroblasts were seeded into 24-well plates (Nunc) at 30,000 cells in complete medium. After 24 hours cells were quiesced in SFM for 24 hours then incubated in either SFM, complete medium (GM), 5ng/ml VEGF-A_{165}a, 20ng/ml VEGF-A_{165}a +/- 10ng/ml *sflt* in SFM, 10ng/ml *sflt* alone, 20ng/ml VEGF-A_{165}b or 20ng/ml VEGF-A_{165}a +20ng/ml VEGF-A_{165}b, in triplicate wells for a further 48 hours. Cells were then trypsinised, stained with Trypan Blue (Lonza) and manual live cell count performed using a haemocytometer.

Wound healing - Migration assay

Fibroblasts were seeded into Ibidi culture chambers (Ibidi GmbH Munich, Germany), in complete culture medium (30,000 cells per chamber) and grown to confluence. Cells were then quiesced for 24 hours in SFM prior to treatment with either SFM alone, complete medium (GM), 20ng/ml VEGF-A_{165}a, 20ng/ml VEGF-A_{165}b or a combination of 20ng/ml VEGF-A_{165}a +20ng/ml VEGF-A_{165}b for 48 hours. Images were taken with the Leica EL6000 digital camera and Image Pro Capture Software with Image J analysis.

High performance liquid chromatography (HPLC)

Fibroblasts were seeded in DMEM/10% FBS at $1x10^5$ cells per well in 6-well plates. After an overnight incubation, the medium was replaced with collagen pre-incubation medium containing 4mM glutamine, 50µg/ml ascorbic acid, 0.2mM proline and 0.4% FBS for 24 hours. Cells were then stimulated with VEGF-A_{165}a, VEGF-A_{165}b or a combination thereof. After a further 24 hours, plates were subjected to a freeze/thaw cycle to lyse cells; the well contents were collected, following scraping of the cell layer, and proteins were precipitated

AJRCCM Articles in Press. Published on 29-June-2017 as 10.1164/rccm.201603-0568OC

with 20% trichloroacetic acid. The protein pellet was spun down, washed with 80% ethanol and air dried prior to hydrolysis with 200µl of 6N HCl at 100°C for 18 hours. An aliquot of acid hydrolysate was dried using a vacuum concentrator and hydroxyproline content was quantified by reverse-phase HPLC following 4-Chloro-7-nitro-1,2,3-benzoxadiazole derivatization; the amount of collagen was calculated assuming that collagen contains 12.2% (w/w) hydroxyproline.

Animal housing and breeding

All experiments were carried out in accordance with the UK Animals (Scientific Procedures) Act 1986 and with approval of the University of Bristol ethical review panel. All mice were housed in pathogen free facilities in line with Home Office regulations in separate cages, in a temperature-controlled room and with alternating 12-hr:12-hr light/dark cycles. Animals were fed a standard diet unless otherwise stated.

Thirty female wild-type (WT) C57Bl6 mice were purchased from Charles River Laboratories (Margate, UK), aged 8-10 weeks. Adult GFP-reporter breeding males ($Rosa^{mT/mG}$) were kindly donated by Dr Richard Coward, University of Bristol.

TG mice constitutively over-expressing VEGF-A_{165}b in the lung (MMTV-$VEGF_{165}b^{+/}$) were generated as previously described. This line was originally generated on a C57Bl6xCBA/CA background then backcrossed with C57/BL6 mice for more than 10 generations (**ref:**E3). Adult female mice were used for all studies and WT littermate controls were used for comparison.

SPC-$rtTA^{+/-}$Tet-O-$Cre^{+/-}$LoxP $VEGF^{+/+}$ mice were generated on a C57Bl6 background by crossing three transgenic mouse lines. LoxP-VEGF: A TG mouse line with LoxP sites inserted around the third exon of VEGF-A (Genentech, San Franscisco, USA). In this mouse, site-specific recombination between LoxP sites results in a null VEGF-A allele (**ref:**E4). A second TG strain carried the target gene, Cre-recombinase, under the regulatory control of a tetracycline-responsive promoter element (Tet-O) and was generated by Dr Andras Nagy and Marina Gertsenstein (Mount Sinai Hospital). In this construct, the target gene is only expressed in the presence of the tetracycline analog, Doxycycline. Finally, heterozygous, male TG mice expressing the reverse tetracycline-controlled transactivator (rtTA) protein under the control of the 3.7 kb human *SFTPC*, surfactant, pulmonary-associated protein C, promoter (SPC mice), were purchased from Jackson Laboratory (Strain Name B6.Cg-Tg(SFTPC-rtTA)5Jaw/J, Stock Number 006235, Bar Harbor, ME). Previous characterisation of this mouse strain has demonstrated that this promoter directs targeted gene expression within ATII cells and the distal conducting airways (**ref**:E5). Upon administration of doxycycline chow (Harlan, TD 01306, 625mg/kg doxycycline hyclate), it was predicted that transcription of the Cre-recombinase was induced only in cells where the rtTA was expressed, initiating site specific recombination between Lox-P sites with deletion of all VEGF-A isoforms, specifically in respiratory ATII cells.

During the breeding of TG mice, genomic DNA (gDNA) was extracted from ear notches of weaned pups and was screened for the existence of transgene by PCR. Details of primers sets and PCR cycling conditions for each transgene are available upon request.

Animal studies

To determine the timing and site specificity of doxycycline-induced Cre recombination in our TG model, $ROSA^{mT/mG+/+}$ reporter mice were bred with $S^{+/-}TC^{+/-}LoxP^{+/-}$

mice (GFP-STCL). The TG construct consists of LoxP flanked fluorescent tomato protein (mT) upstream of Green Fluorescent Protein (GFP), under the control of a chicken beta actin promoter (pCA). When bred to Cre recombinase expressing TG mice, the mT cassette is deleted in *Cre* expressing tissues of the resulting offspring, allowing expression of the membrane-targeted GFP (mGFP) cassette located immediately downstream. GFP-STCL mice (n=5) and littermate controls (n=5) were induced with doxycycline chow (Harlan, TD 01306, 625mg/kg doxycycline hyclate) for a minimum period of 10 weeks. During this induction period, anaesthetised mice were imaged for the presence of GFP-lung fluorescence, using an IVIS Spectrum whole animal *in vivo* imaging system (Xenogen, Hopkinton, MA), initially at 4 weeks and then every 2 weeks thereafter. Mice were imaged lying prone, in addition to on their left and right sides.

To maximise the GFP-fluorescent signal, hair was removed from the thoracic area of each mouse using depilatory cream (Nair, Church & Dwight) prior to imaging. One control and one experimental mouse were imaged simultaneously and the acquired images were analysed using Live Image software (version 2.5), normalising for auto-fluorescence from the animal body itself to provide a quantitative fluorescent signal. Upon detection of GFP-lung fluorescence by IVIS imaging, the presence of GFP fluorescence was confirmed by direct visualisation of sectioned lung tissue.

Lung samples from GFP reporter mice were embedded and frozen in (TissueTek), prior to sectioning (5μm, Superfrost slides). The liver and kidneys were also prepared in the same way to provide tissue controls. For direct immunofluorescence sections were fixed in 4% PFA, washed in 1XPBS then mounted with coverslips using Vectashield mountant containing DAPI (Vectashield, H-1200). Slides were imaged using Leica EL6000 digital camera and Leica Application Suite Advanced Fluorescent (LASAF) software.

In situ hybridisation

Dissected lung samples for *in-situ* hybridisation were fixed in 4% PFA overnight (Alfa Aesar) at room temperature (RT), then immersed in 30% sucrose in PBS. Lungs were snap frozen in OCT (Sakura) and sectioned at 5μm onto poly-l-lysine slides (Sigma) and stored at -80°C.

Slides were air-dried then treated with 15μg/ml Proteinase K (Sigma P2308). Slides were washed Hyclone-PBS (Thermo-Scientific) and then then fixed in 4% PFA prior to sequential washing in DEPC-PBS and 2xSSC (Roche) (pH7).Sections were pre-hybridised in pre-heated hybridisation buffer in a 50% Formamide (Roche)/5xSSC humidified chamber, and incubated overnight at 60°C with sense (negative control) and anti-sense VEGF-A RNA probes (1μg/ml)(kind gift from S. Quaggin).

The following day, slides were rinsed in 2 x SSC, followed by washes in 50% formamide/0.2% x SSC. Sections were then washed twice in 2 x SSC, followed by a 5 minute wash in NT buffer (pH7.5). Sections were incubated in NT blocking buffer prior to the addition of an anti-DIG AP Fab fragment antibody (Roche). Slides were washed twice in TBSTL then in APB buffer. BM purple AP colour substrate (Roche) was applied to sections, slides wrapped in foil and incubated in a humidified chamber overnight. The following day slides were washed in dH_2O prior to immersion in Nuclear Fast Red (Vector) counterstain .Slides were rinsed in tap water then dehydrated through increasing concentrations of ETOH and cleared in xylene. Sections were mounted with DPX mountant (Sigma) and coverslips prior to imaging.

Bleomycin-induced model of pulmonary fibrosis

AJRCCM Articles in Press. Published on 29-June-2017 as 10.1164/rccm.201603-0568OC

The Bleomycin-induced murine model of pulmonary fibrosis was used to investigate the possible role of VEGF-A in lung fibrogenesis. Mice (10-12 weeks) were anaesthetised with inhalation of 2% isoflurane prior to the administration of Bleomycin (50IU per mouse in 50μL sterile 0.9% Saline, Bleo-Kyowa; gift from Kyowa Hakko Ltd, Slough, UK) or an equivalent volume of sterile 0.9% Saline vehicle, by an oro-phrayngeal instillation technique (**ref:**E6). Adult SPC-rtTA$^{+/-}$Tet-O-Cre$^{+/-}$LoxP VEGF$^{+/+}$ mice (6-8 weeks old) received doxycycline chow for 12 weeks (TD 01306, 625mg/kg doxycycline hyclate, Harlan, UK) prior to the administration of BLM. Body weight and well-being was monitored on alternate days. Mice were culled at 21 days by Schedule 1 methods and samples harvested. The lungs were lavaged using 3 x 1ml instillations of 0.9% sterile Saline, each withdrawn via an intra-tracheal catheter (22 Gauge, Bioflon). Lavage fluid was centrifuged at 13,000 rpm for 5 minutes to clear cells, the supernatant was removed then stored at -80^{o}C.

The heart and lungs were removed *en-bloc*. The right lung was tied off and snap frozen in liquid nitrogen, whilst the left lung was inflated under gravity with 10% neutral-buffered formalin (Sigma), incubated in the same solution overnight at 4^{0}C, prior to paraffin wax embedding and sectioning (5μm, Superfrost slides).

Determination of lung fibrosis

Lung fibrosis was assessed histologically by Masson's Trichrome staining and lung fibrosis score. Quantification of lung fibronectin and pro-collagen-1α mRNA expression provided additional supportive information.

Masson's Trichrome staining

Slides were de-waxed in Xylene (Sigma) for 6 mins prior to rehydration of tissue in decreasing concentrations of Ethanol. The slides were rinsed in dH_2O, then allowed to mordant in Bouin's Solution (Sigma) overnight in a fume extraction hood. Slides were washed in running tap water and then rinsed in dH_2O.,then immersed in Weigert's Iron Haematoxylin (made fresh by adding equal volumes of Solution A (1% Haematoxylin in 95% ETOH) and Solution B (1.2% Ferric Chloride and 1% Acetic Acid in dH_2O)(Sigma), staining nuclei blue-black. Slides were washed and rinsed in de-ionised water prior to immersion in Biebrich Scarlet-Acid Fuchsin stain (Sigma, Accustain Trichrome stain kit, 0.9% Biebrich scarlet, 0.1% Acid Fuchsin and 1% Acetic Acid) for 5 minutes, staining cytoplasm and muscle red. The slides were washed in dH_2O and immersed in freshly prepared Phosphotungstic / Phosphomolybdic Acid Solution (1:1 volume)(Sigma, Accustain Trichrome stain kit, 10% Phosphotungstic Acid and Phosphomolybdic Acid solution), providing the acidic environment required for uptake of the Aniline Blue stain. Sections were then stained in Aniline Blue (Sigma, Accustain Trichrome stain kit, 2.4% Aniline Blue, 2% Acetic Acid), staining collagen blue. Slides were rinsed in dH_2O prior to immersion in 1% Acetic Acid solution (Fischer Scientific) to differentiate the blue stain and then rapidly dehydrated before clearing in Xylene and mounting pre-analysis.

Lung fibrosis Score

The fibrosis score of each mouse lung was evaluated from H&E stained lung sections by two blinded observers, one independent to the project. Twenty (x40 magnification) non-overlapping fields of view were assessed per section for the presence of alveolar wall thickening: 1 = <25%, 2 = 25-50%, 3 = 50-75%, 4= 75-100% of field affected). Only fields composed predominantly of alveoli were quantified.

Statistical analysis

Statistical analysis was performed using Graph Pad Prism software (Version 5.0). For the analysis of two groups the unpaired *t*-test was used, with or without Welch's correction dependent on the variance of data between groups. ANOVA with post-hoc Holm's Sidak multiple comparisons analysis was used for multiple group comparisons. For all tests a $p < 0.05$ was considered statistically significant. Data presented as means with SEM.

References:

E1 Jenkins, R.G., et al., Longitudinal change in collagen degradation biomarkers in idiopathic pulmonary fibrosis: an analysis from the prospective, multicentre PROFILE study. *Lancet Respir Med,* 2015. **3**(6): p. 462-72.

E2 Varey, A. H. *et al.* VEGF 165 b, an antiangiogenic VEGF-A isoform, binds and inhibits bevacizumab treatment in experimental colorectal carcinoma: balance of pro- and antiangiogenic VEGF-A isoforms has implications for therapy. *British journal of cancer* **98**, 1366-1379, (2008).

E3. Qiu, Y. *et al.* Mammary alveolar development during lactation is inhibited by the endogenous antiangiogenic growth factor isoform, VEGF165b. *FASEB J* **22**, 1104-1112, (2008).

E4. Gerber, H. P. *et al.* VEGF is required for growth and survival in neonatal mice. *Development* **126**, 1149-1159 (1999).

E5. Perl, A. K., Zhang, L. & Whitsett, J. A. Conditional expression of genes in the respiratory epithelium in transgenic mice: cautionary notes and toward building a better mouse trap. *American journal of respiratory cell and molecular biology* **40**, 1-3, (2009).E6. Scotton, C. J. *et al.* Ex vivo micro-computed tomography analysis of bleomycin-induced lung fibrosis for preclinical drug evaluation. *The European respiratory journal* **42**, 1633-1645, (2013).

Figure E 1: Sequencing chromatograms of products obtained by RT-PCR of human normal and IPF lung RNA extracts. Gel bands were initially digested then analysed by direct sequencing. Using VEGF-A Exon 8b reverse primers, products consistent with a) VEGF-A_{121}a b) VEGF-A_{165}a and c) VEGF-A_{189}a were sequenced. Using a VEGF-A Exon 7a forward primer, the gel product from IPF Patient 3 confirmed the expression of VEGF-A_{165}b (d).

Figure E 2: Expression of VEGF-A isoforms in normal and IPF lung

a) Patient demographics of IPF and control groups for BALF data in Figure 1e. Groups were statistically comparable (unpaired *t*-test, IPF group n=15, healthy control group n=13). b) PanVEGF-A and VEGF-A_{165}b immunohistochemical staining: Lower magnification of images shown in Figure 1f. Intense staining of the alveolar epithelium was observed for both panVEGF-A and VEGF-A_{165}b in normal and IPF lungs (block arrows). Additional sites of localisation included vessel walls (open arrow heads), fibroblasts (FFo indicates the fibrotic focus), lymphocytes and alveolar macrophages (AM). Isotype IgG shown as negative control. Scale bar =25μm original magnification x40.

Figure E3A: Expression of VEGFR1, VEGFR2, NP1 and NP2 in the normal and IPF lung

AJRCCM Articles in Press. Published on 29-June-2017 as 10.1164/rccm.201603-0568OC

VEGF-A receptor and co-receptor immunohistochemical staining: Intense staining of the alveolar epithelium was observed for VEGFR1, VEGFR2, NP1 and NP2 (arrows) in both the normal and IPF lung. Additional sites of localisation included the vascular endothelium, fibroblasts (FFo indicates the fibrotic focus), lymphocytes and alveolar macrophages (AM). Isotype IgG shown as negative control. Scale bar=10μm, original magnification x100.

Figure E 3B: Co-staining of VEGFR1 and VEGFR2 with E-cadherin in a) normal lung and b) IPF lung.
E-Cadherin co-localised with both VEGFR1 and VEGFR2 to the alveolar epithelium in normal lung (arrows) In the IPF lung E-Cadherin staining was heterogeneous but again co-localised with VEGFR1 and VEGFR2 (arrows)(arrowheads) (n=3, n=1 shown). Original magnification of images x100 (scale bar = 10μm).

Figure E 3C: Expression of VEGFR1, VEGFR2, NP1 and NP2 in NF and FF by qRT-PCR
a) NF and FF expressed the key VEGF-A receptors and co-receptor mRNA at comparable levels by qRT-PCR (data presented as means with SEM, NF: n=5, FF: n=6, unpaired *t*- test).
b) Sequencing chromatograms of products obtained from qRT-PCR of NF and FF cell culture RNA extracts. Receptor specific forward primers were used as the template to amplify each target sequence of interest. Sequencing confirmed the amplification of VEGFR1, VEGFR2, NP1 and NP2 in NF and FF cell extracts (NF n=2, FF n=2 for each product, n=1 shown).

Figure E 4: Densitometric analysis of phosphorylation of MEK and p42/p44 proteins in NF and FF in response to VEGF-A_{165}a or VEGF-A_{165}b treatment. Representative western blots shown in Figure 3. Increased phosphorylation of MEK and p42/p44 was observed in response to VEGF-A_{165}a and VEGF-A_{165}b in both NF and FF compared to SFM (data presented as means with SEM, n=3,*p<0.05, **p<0.01, unpaired *t*-test).

Figure E 5: RT-PCR of VEGF-A isoform expression in NF and FF using Exon2/3 forward primer and 8b reverse primer a) Map of exon structures of several of the VEGF-A isoforms with predicted isoform length. Arrows indicate panVEGF-A primer positions. b) Agarose gel electrophoresis following RT-PCR demonstrating the amplification of at least two isoforms. c) The prominent bands produced were excised and sequenced using the 8b reverse primer, confirming the amplification of VEGF-A_{165}a and VEGF-A_{121}a.

Figure E 6: RT-PCR of VEGF-A isoform expression in NF and FF using Exon 7a forward primer and 8b reverse primer a) Map of exon structures of VEGF-A_{165}a and VEGF-A_{165}b isoforms with predicted isoform length. Arrows indicate primer positions. b) RT-PCR of RNA extracted from NF (n=5) and FF (n=6) cultures using VEGF-A Exon 7a forward and Exon 8b reverse primers. Two bands were observed consistent with the expression of both proximal (VEGF-A_{165}a ~ 195bp) and distal splice isoforms (VEGF-A_{165}b ~ 129bp). Plasmids containing VEGF-A_{165}a and VEGF-A_{165}b were used as positive controls (alone and mixed in a 1:1 ratio). L indicates 100bp marker. c) The prominent bands produced were excised and sequenced using the 7a forward primer, confirming the amplification of VEGF-A_{165}a and VEGF-A_{165}b. Exons 7 and 8a are highlighted on the sequencing chromatogram of the195bp PCR product (Top Band): Codons translated to give the terminal six amino acids expected for isoforms of the VEGF-A_{xxx}a family (Cysteine-Aspartic acid-Lysine-Proline-Arginine-Arginine). Exons 7 and 8b are highlighted on the sequencing chromatogram of the129bp PCR product (Bottom band): The highlighted sequence corresponds to Codons translated to give the terminal six amino acids specific to the VEGF-A_{xxx}b family of isoforms (Serine-Leucine-Threonine-Arginine-Lysine-Aspartic acid).

Figure E 7: VEGF-A isoform expression in NF and FF.

Quantitative RT-PCR of NF and FF (n=5) panVEGF-A and VEGF-A_{xxx}b isoform mRNA. No significant differences in the mRNA levels of panVEGF-A or VEGF-A_{xxx}b isoforms were detected between NF and FF (unpaired *t*-test).

Figure E 8: Cell immunofluorescence of panVEGF-A and VEGF-A_{165}b expression in NF and FF. Comparable patterns were observed for NF and FF, with cytoplasmic and perinuclear expression of panVEGF-A and cytoplasmic expression of VEGF-A_{165}b. Primary antibody shown in green, Phalloidin (F-actin) in red and DAPI (nuclear) in blue, with an overlay image of all three stains. Isotype IgG controls were used as negative controls. Images taken at x40 magnification with scale bar indicating 25μm.

Figure E 9: Fibroblast wound healing in response to VEGF-A_{165}a and VEGF-A_{165}b. VEGF-A_{165}a and VEGF-A_{165}b significantly increased the migration of NF at 48 hours (*$p<0.05$). This effect was blocked by the concomitant treatment of VEGF-A_{165}a and VEGF-A_{165}b. Recombinant VEGF-A proteins had no significant effect on the migration of FF. Representative images of n=4, Scale bar 80μm, original magnification x10.).

Figure E 10: Kidney and Liver sections from GFP-STCL mice : A GFP-reporter mouse ($ROSA^{mT/mG}$) was crossed with $SPC^{+/-}$-$TC^{+/-}$-$LoxP^{+/-}$ mice to determine the tissue specificity of Cre-recombinase activity following doxycycline induction. These mice possess LoxP sites on either side of a membrane-targeted tdTomato (mT) cassette and express red fluorescence in all tissues. In the presence of Cre recombinase, the mT cassette is deleted allowing expression of the membrane-targeted EGFP (mG) cassette located just downstream. Visualisation of kidney and liver sections of doxycycline-induced GFP-STCL mice demonstrated an absence of GFP fluorescence at both 12 and 14 weeks (12 week images shown, images taken at x40 magnification, scale bar 25μm, n=3, n=1 shown, DAPI (nuclear) counterstain).

Figure E 11: Phenotype of MMTV-VEGF-A_{165}b mice. a) RT-PCR using primers specific for a) human panVEGF-A and b) the MMTV-VEGF-A_{165}b transgene comparing transgenic (TG) mice to littermate controls (WT). Bands consistent with detectable human VEGF-A_{165}b (i) and the MMTV-VEGF-A_{165}b transgene (ii) in TG mice. b) H&E stained lung sections of TG mice and WT littermate controls. MMTV-VEGF-A_{165}b (TG) mice demonstrated normal parenchymal architecture and pulmonary vasculature. Images taken at x10 magnification, scale bar 100μm (a+c) and at x40 magnification, scale bar 25μm (b+d).

AJRCCM Articles in Press. Published on 29-June-2017 as 10.1164/rccm.201603-0568OC

Table E 1:Table of primer sequences for human RT-PCR reactions

Primer name	Sequence
Human VEGFR1	**For** : 5'- GAGCTCCCTTCCTTCAGTCA-3'
	Rev: 5'-GAAGAAGGAGGCAGAATCTGCAA-3'
Human VEGFR2	**For**: 5'-AGAATGGAAGAGGATTCTGG-3'
	Rev: 5'-CGGCTCTTTCGCTTACTGTT-3'
Human NP1	**For**: 5'-CCCCGGGTACCTTACATCTC-3
	Rev: 5'-TGCAGTCTCTGTCCTCCAAA-3'
Human NP2	**For**: 5'-GAACTGCATGGAACCCATCT-3'
	Rev: 5'-CCCTGAGGTTGCAGAAGAAG-3'
Human PanVEGF (exon2/3) RT-PCR	**For**: 5'-CGA AGT GGT GAA GTT CAT GGAT G-3'
Human PanVEGF (exon 7a) RT-PCR	**For**: 5'-GTTTGTACAAGATCCGCAGACGT-3'
Human PanVEGF (exon 7b) qPCR	**For**: 5'–CGTTGCAAGGCGAGGCAGC-3'
Human PanVEGF (3'UTR of exon 8b) qPCR+RTPCR	**Rev**: 5'-TTCTGTATCAGTCTTTCCTGGTGA-3'
Human VEGFxxx only (exon 7a) qPCR	**For**: 5'-TTGCTCAGAGCGGAGAAAGC-3'
(exon 8a) qPCR	**Rev**: 5'-TCACCGCCTCGGCTTGTCACAT-3'
Human Fibronectin	**For**: 5'-ACCTAGGATGACTCGTGCTTTGA-3'
	Rev: 5'-CAAAGCCTAAGCACTGGCACAACA-3'
Human β-Actin	**For:** 5'-AGA AGG ATT CCT ATG TGG GCG-3'
	Rev: 5'-CAT GTC GTC CCA GTT GGT GAC-3'

Table E 2: Table of primer sequences for murine RT-PCR reactions

Primer name	Sequence
Murine Fibronectin	For: 5'-AAA CTT GCA TCT GGA GGC AAA CC-3' Rev: 5 '-AGC TCT GAT CAG CAT GGA CCA CT-3'
Murine pro-Collagen-1α	For: 5'-GCAACAGTCGCTTCACCTACA-3' Rev: 5'-CAATGTCCAAGGGAGCCACAT-3'
Murine panVEGF-A	For: 5'-GGC TAT AAG TTC TTT GCT GAC CTG-3' Rev: 5'-AAC TTT TAT GTC CCC CGT TGA-3'
Murine HPRT (qPCR)	For: 5'-GGC TAT AAG TTC TTT GCT GAC CTG-3' Rev: 5'-AAC TTT TAT GTC CCC CGT TGA-3'

AJRCCM Articles in Press. Published on 29-June-2017 as 10.1164/rccm.201603-0568OC

Supplementary Figure 1

a)

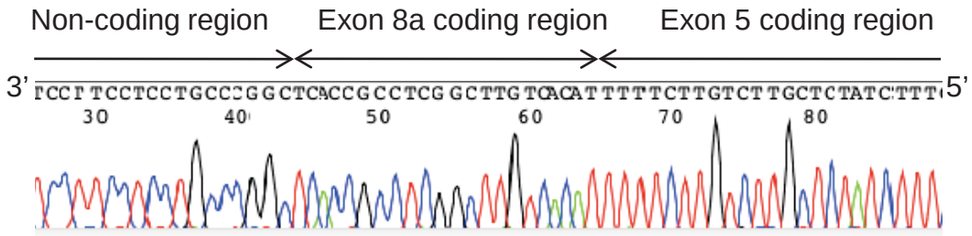

b)

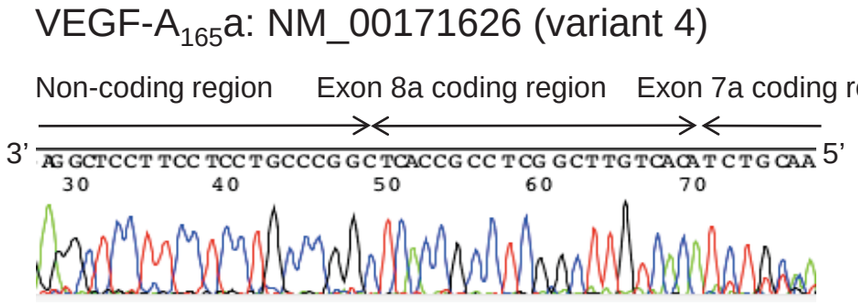

c)

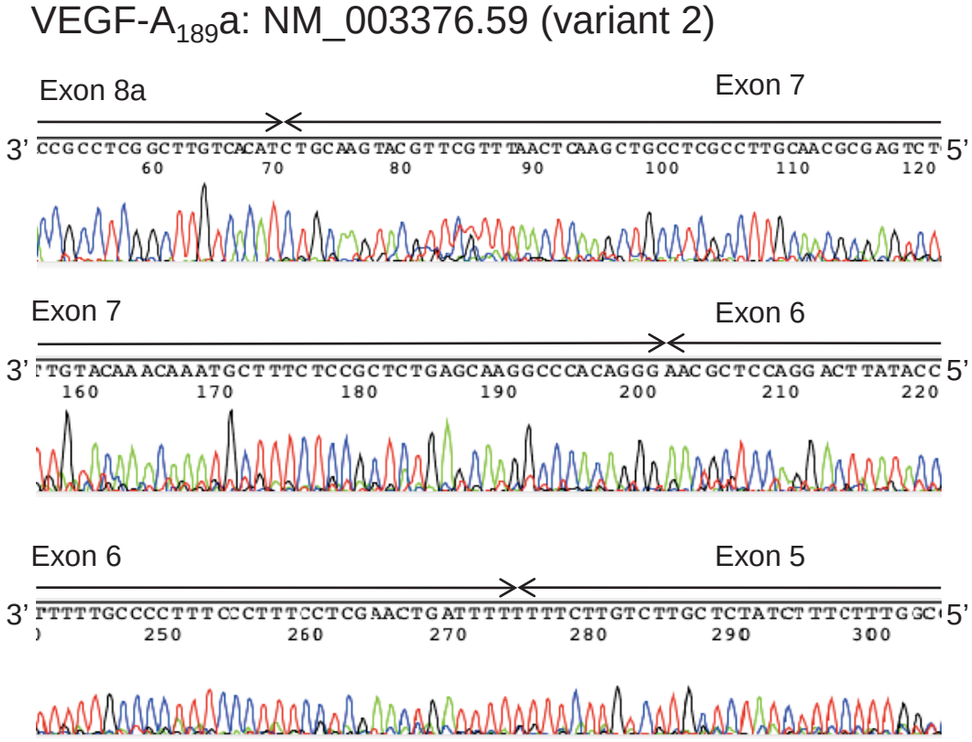

d)

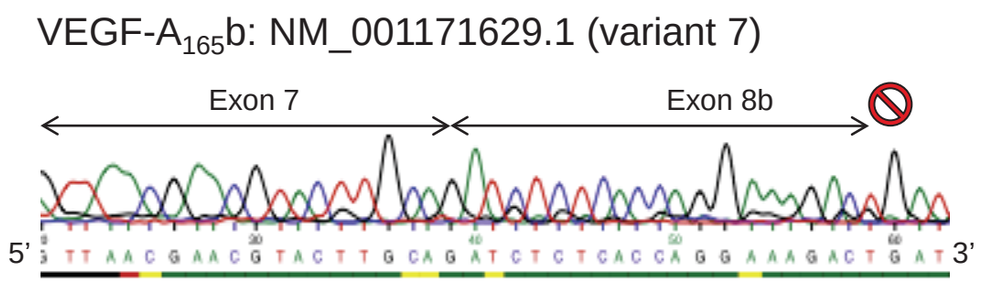

Supplementary Figure 2

a)

	Controls	IPF
Age	60.5 (+/-16.1)	66.5(+/-10.6)
Gender	10M:3F	10M:5F

b)

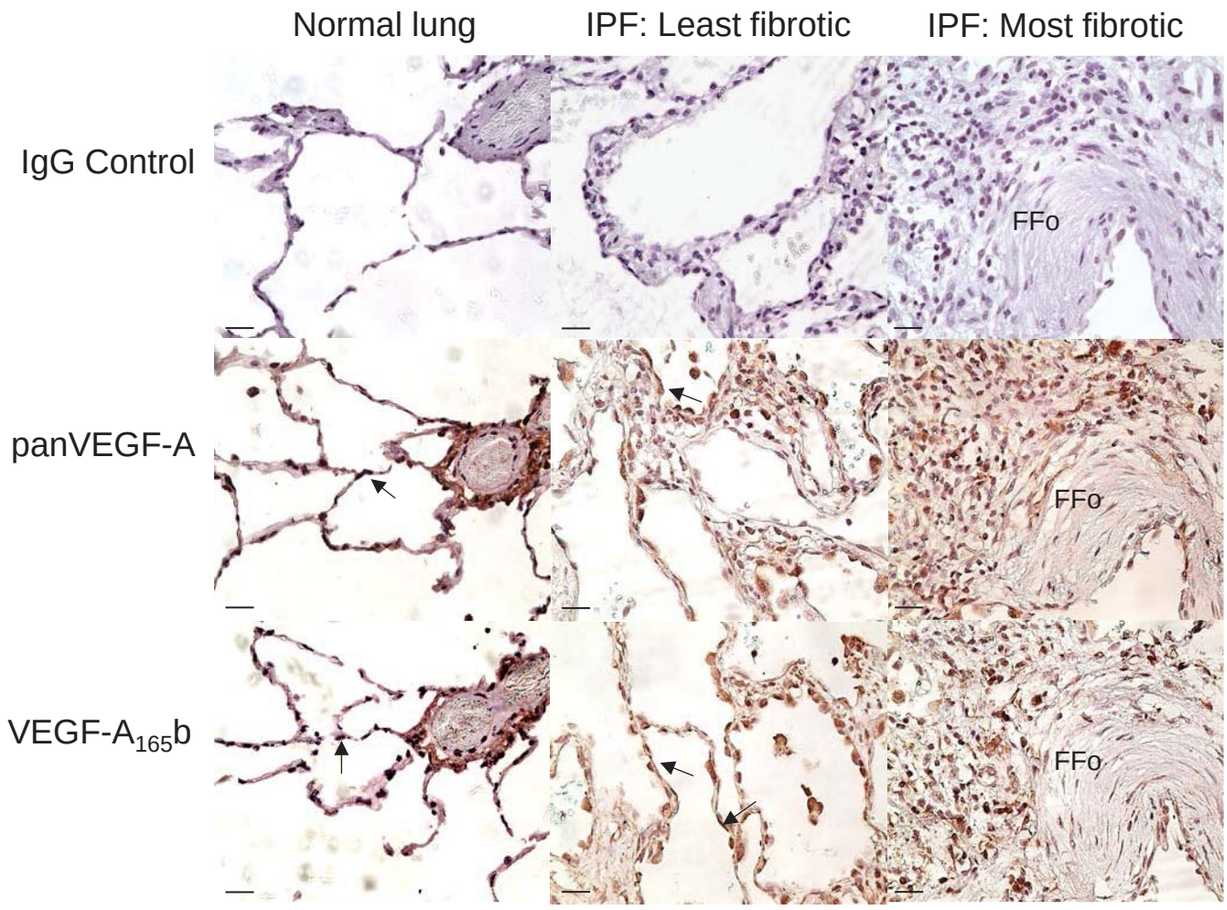

AJRCCM Articles in Press. Published on 29-June-2017 as 10.1164/rccm.201603-0568OC

Supplementary Figure 3A

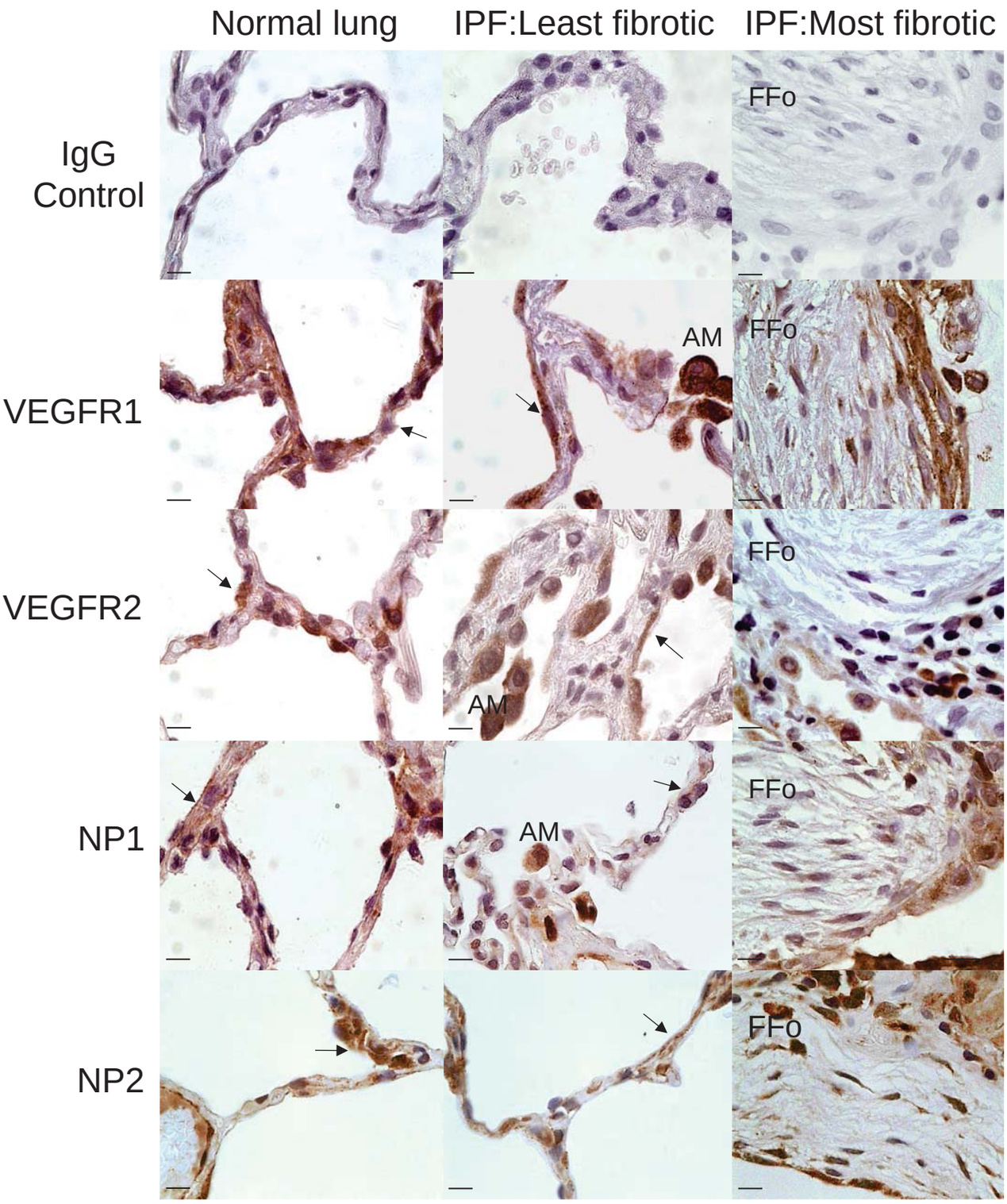

Supplementary Figure 3B

a) Normal Lung

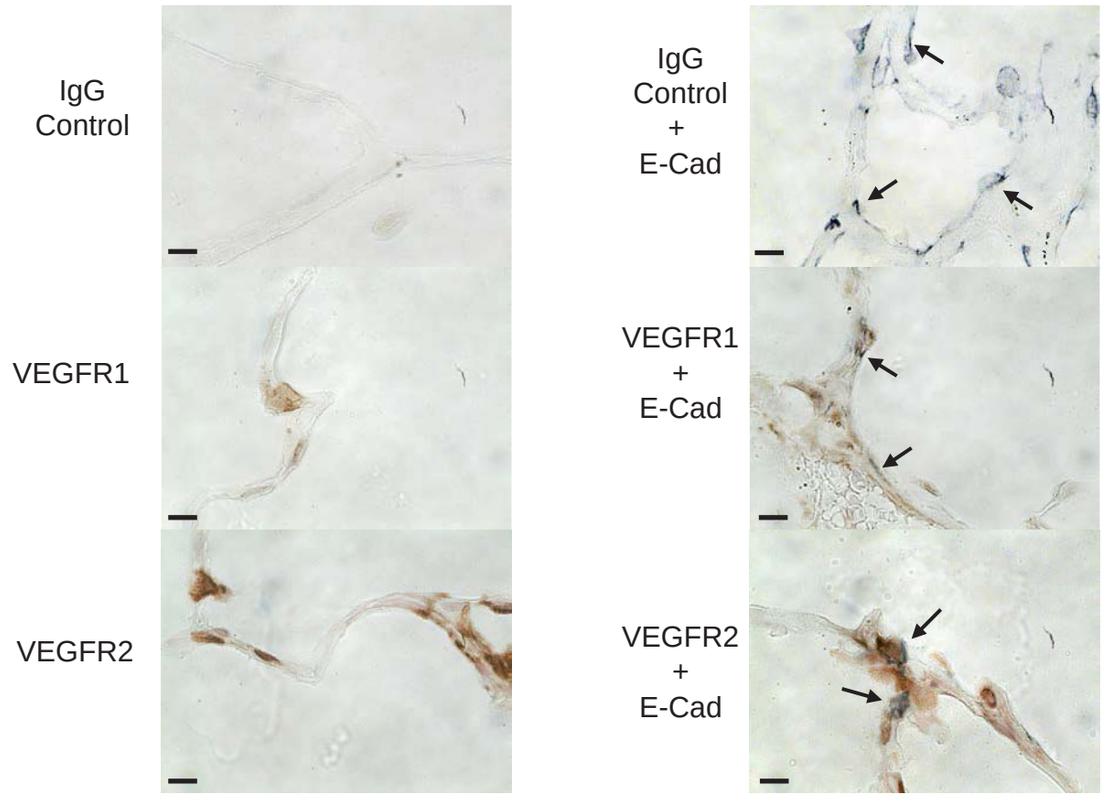

b) IPF Lung

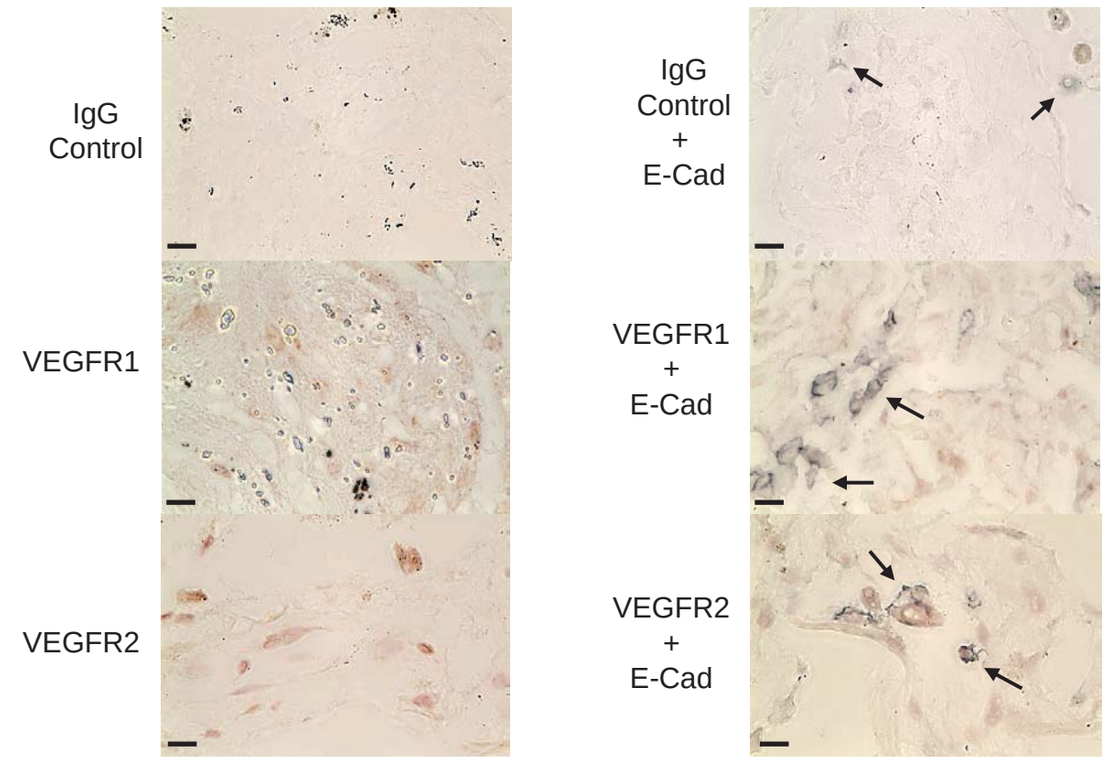

AJRCCM Articles in Press. Published on 29-June-2017 as 10.1164/rccm.201603-0568OC

Supplementary Figure 3C

a)

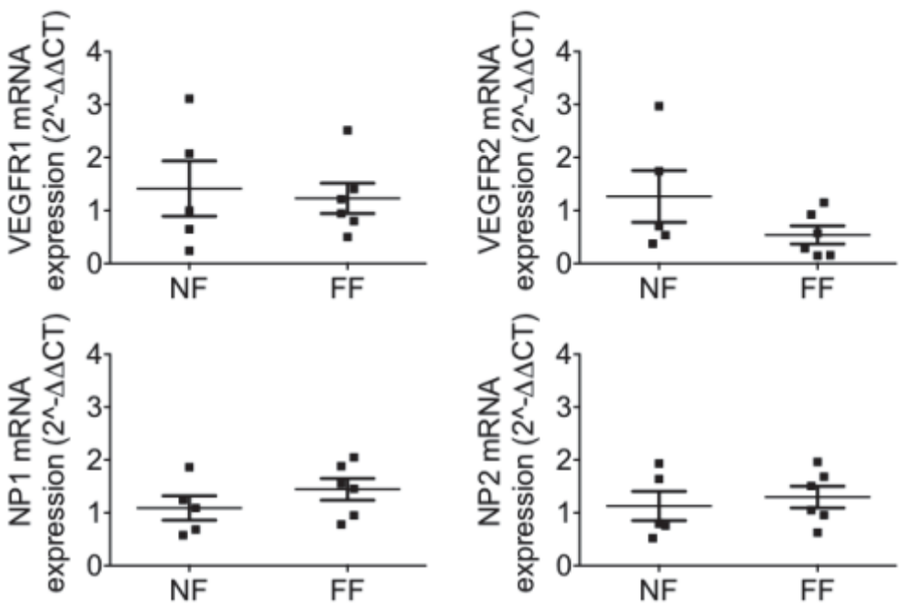

b)

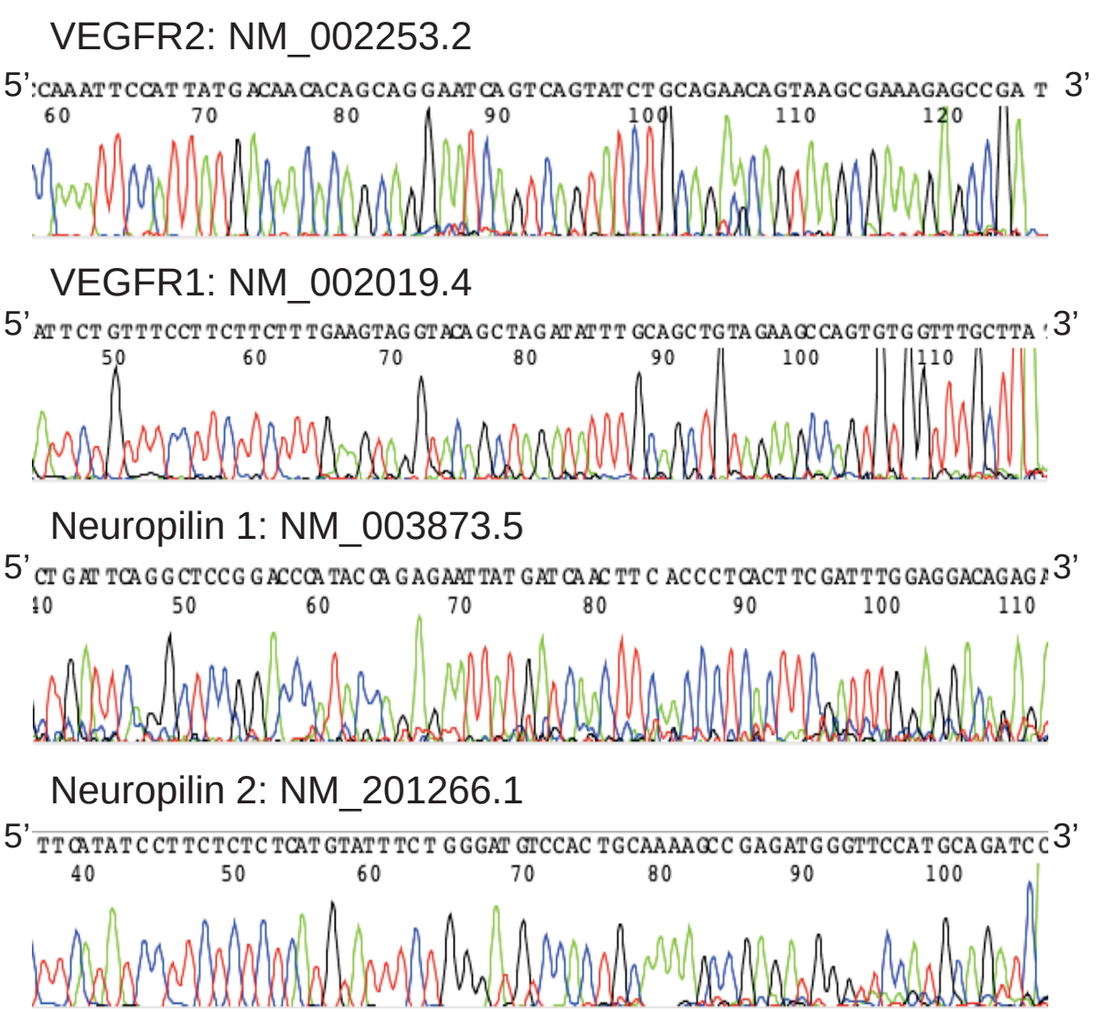

Supplementary Figure 4

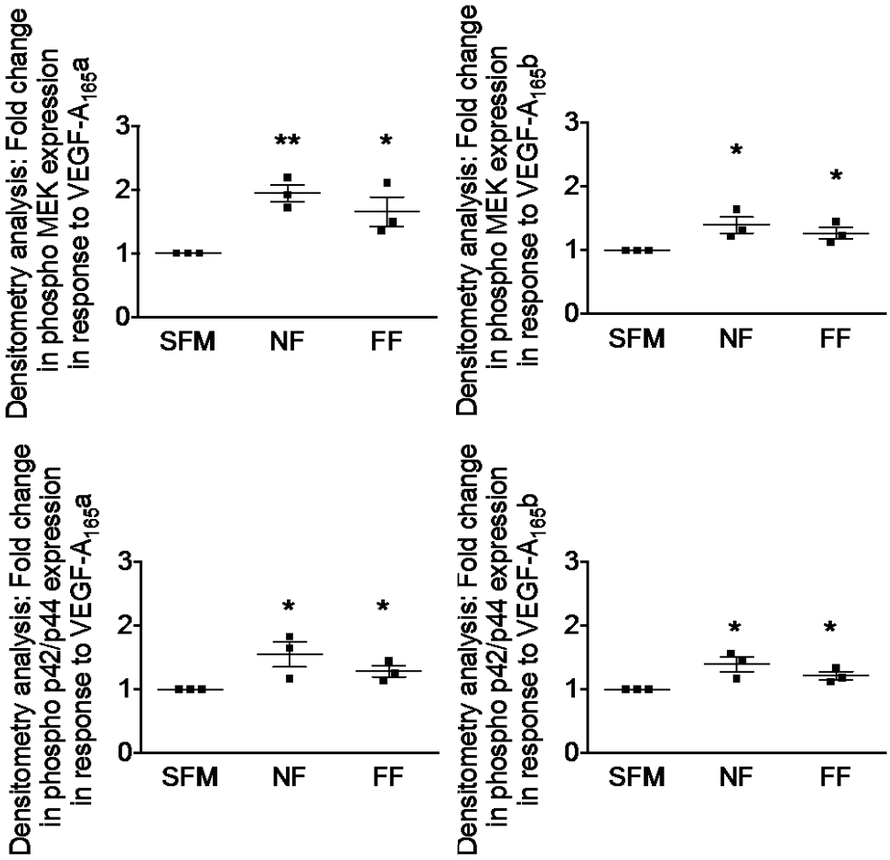

AJRCCM Articles in Press. Published on 29-June-2017 as 10.1164/rccm.201603-0568OC

Supplementary Figure 5

a)

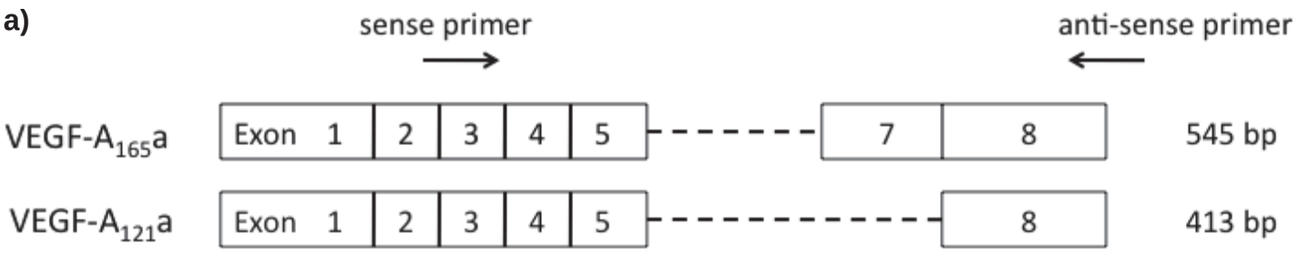

b)

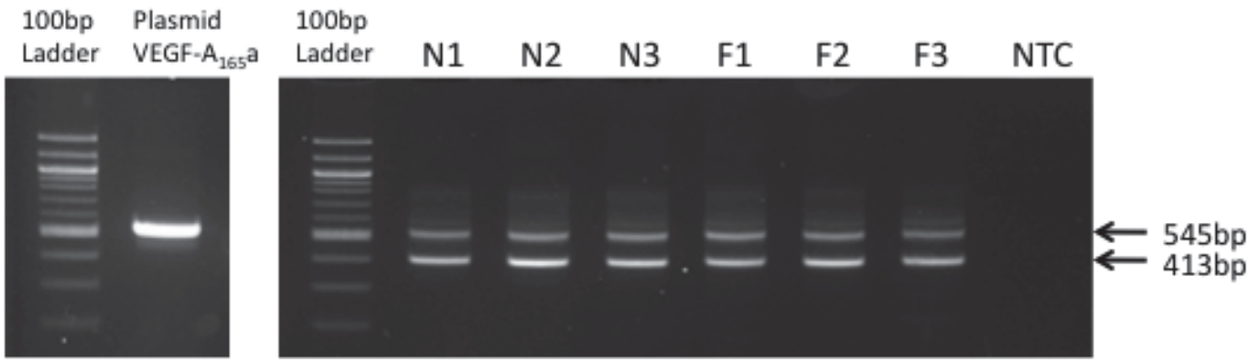

N: Normal Fibroblast
F: Fibrotic Fibroblast
NTC: Non Template Control

c)

Band at 545bp: VEGF-A_{165}a, NM_00171626 (variant 4)

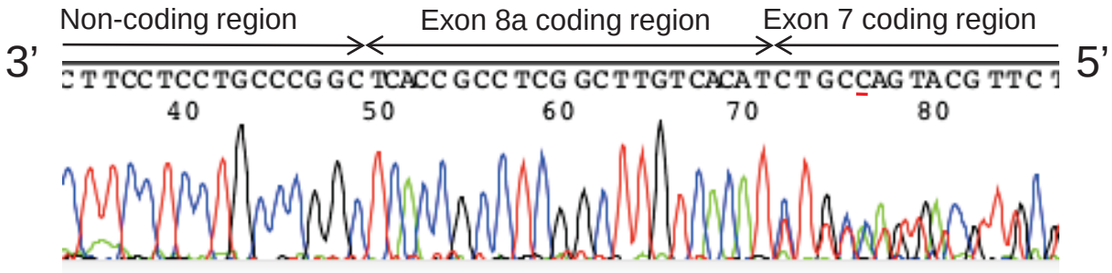

Band at 413bp: VEGF-A_{121}a, NM_001171628.1 (variant 6)

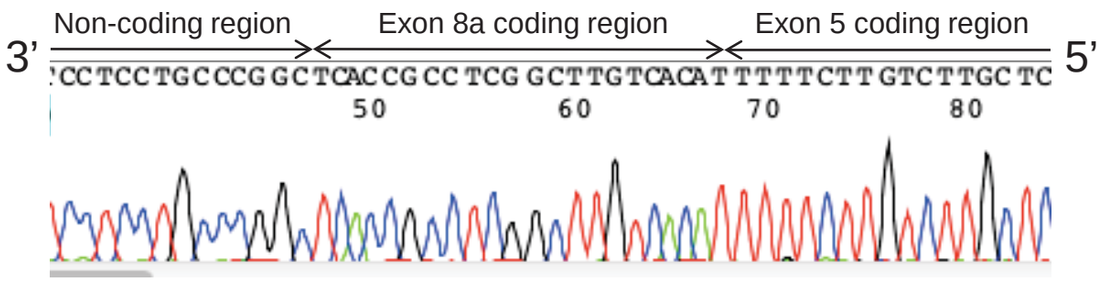

Supplementary Figure 6

a)

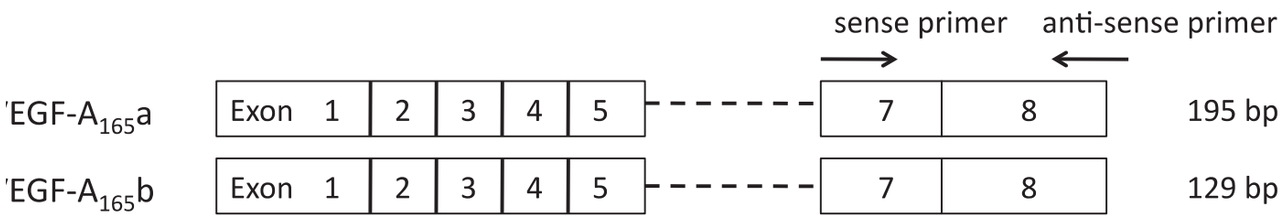

b)

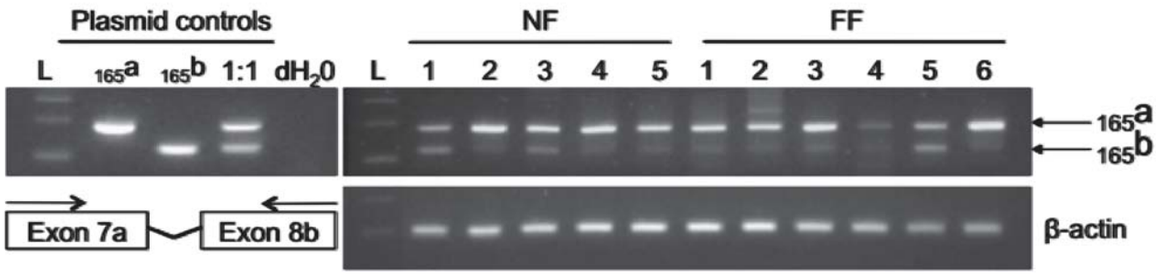

c)

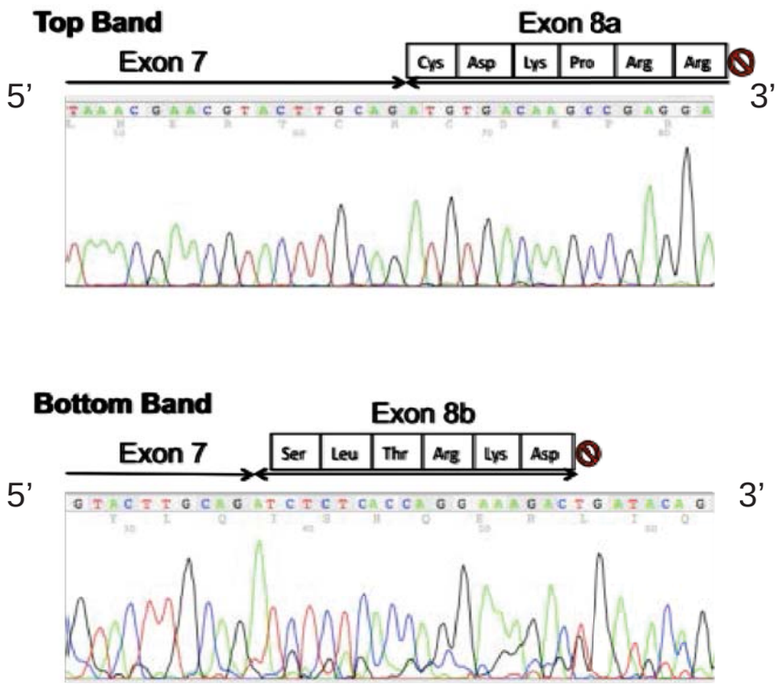

AJRCCM Articles in Press. Published on 29-June-2017 as 10.1164/rccm.201603-0568OC

Supplementary Figure 7

a)

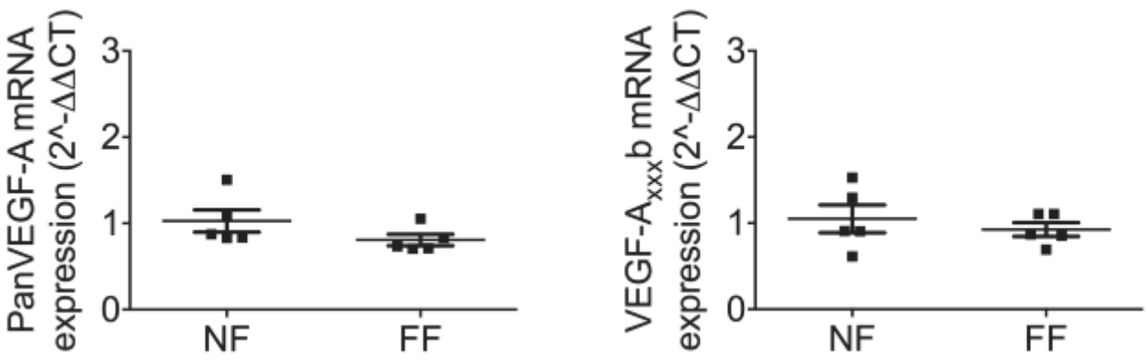

Supplementary Figure 8

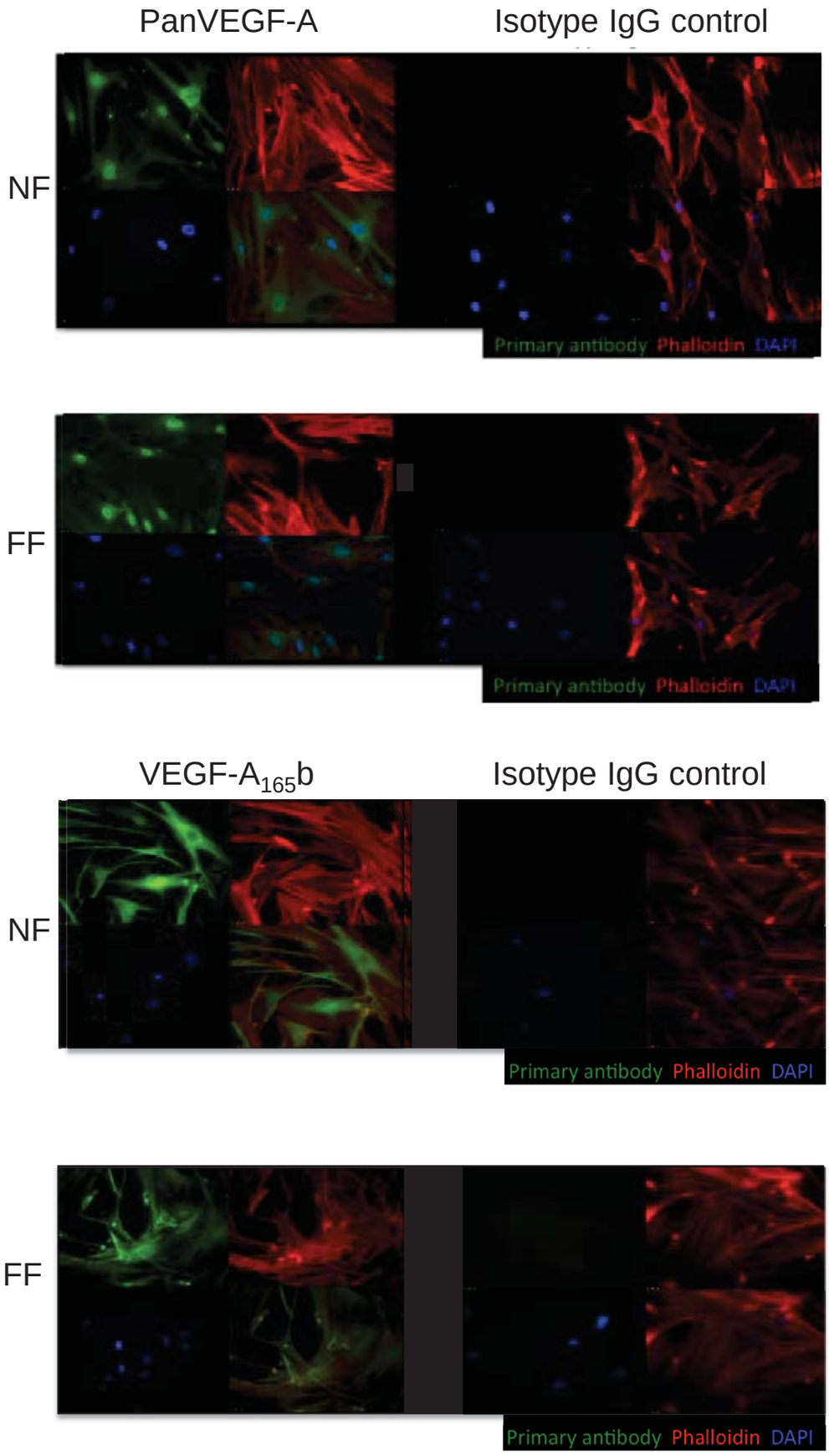

AJRCCM Articles in Press. Published on 29-June-2017 as 10.1164/rccm.201603-0568OC

Supplementary Figure 9

a) Normal Fibroblasts

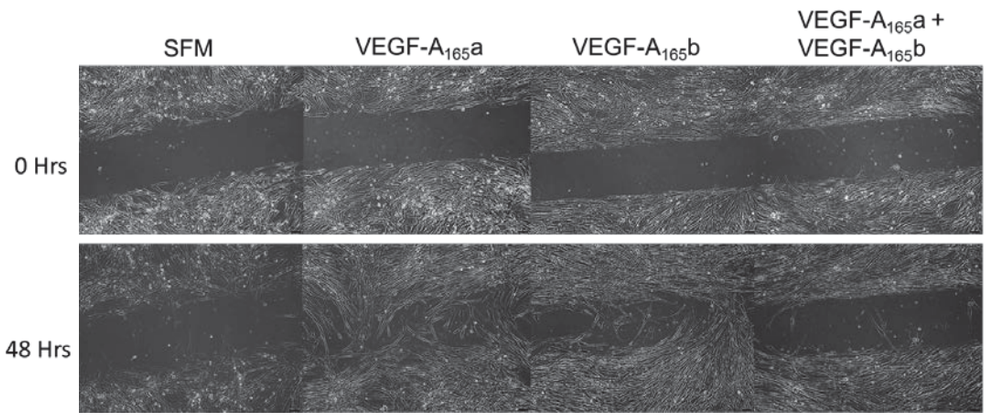

b) Fibrotic fibroblasts

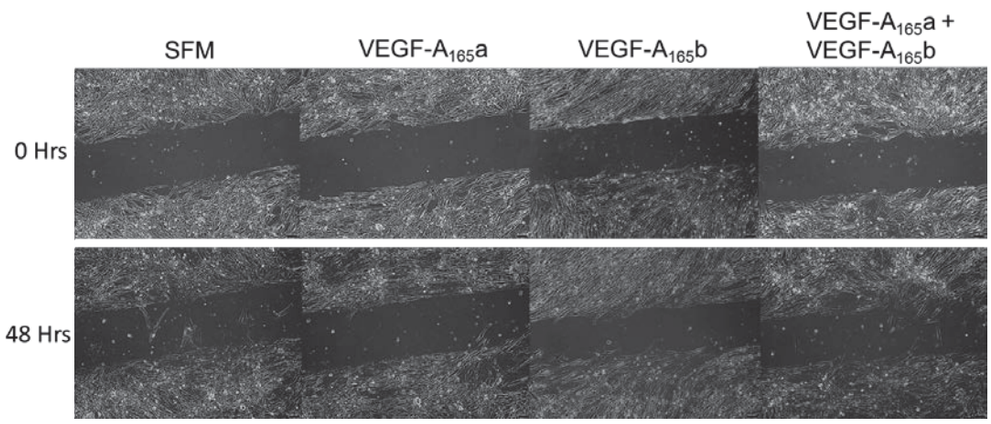

AJRCCM Articles in Press. Published on 29-June-2017 as 10.1164/rccm.201603-0568OC

Supplementary Figure 10

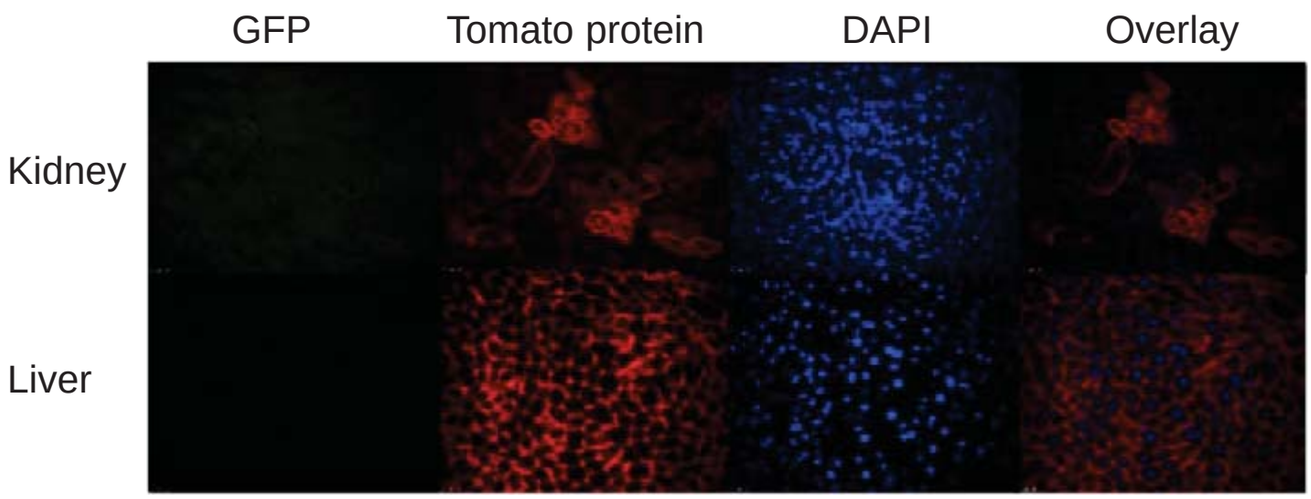

AJRCCM Articles in Press. Published on 29-June-2017 as 10.1164/rccm.201603-0568OC

Supplementary Figure 11

a)

i) Human PanVEGF-A primers (Exon 7a For, 8b Rev)

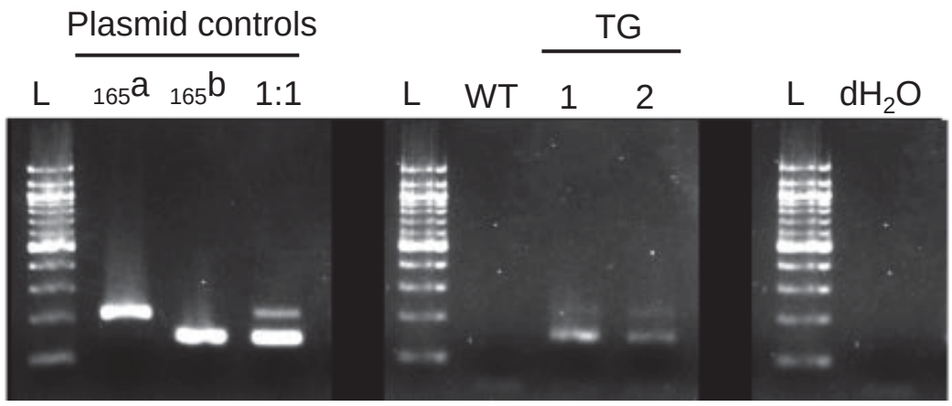

L: Ladder
WT: Wildtype
TG: Transgenic

ii) MMTV-VEGF$_{165}$ transgene primers

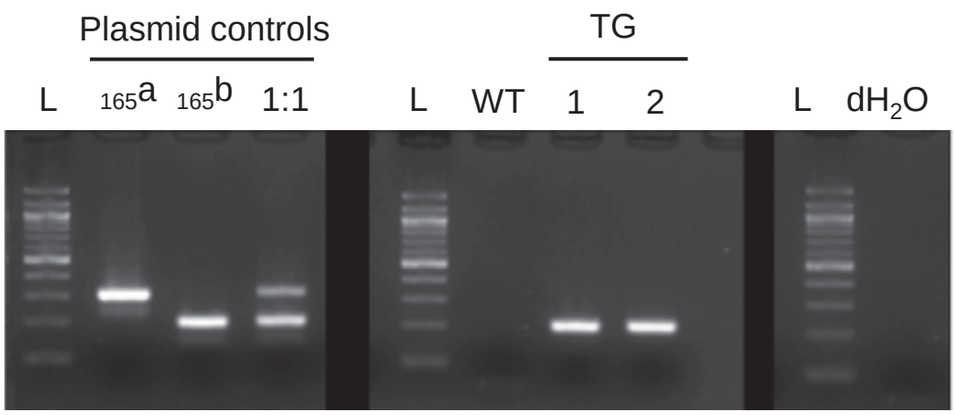

L: Ladder
WT: Wildtype
TG: Transgenic

b)